iScience

CellPress

Article

# Teaching an Old Poly(arylene ether) New Tricks: Efficient Blue Thermally Activated Delayed Fluorescence

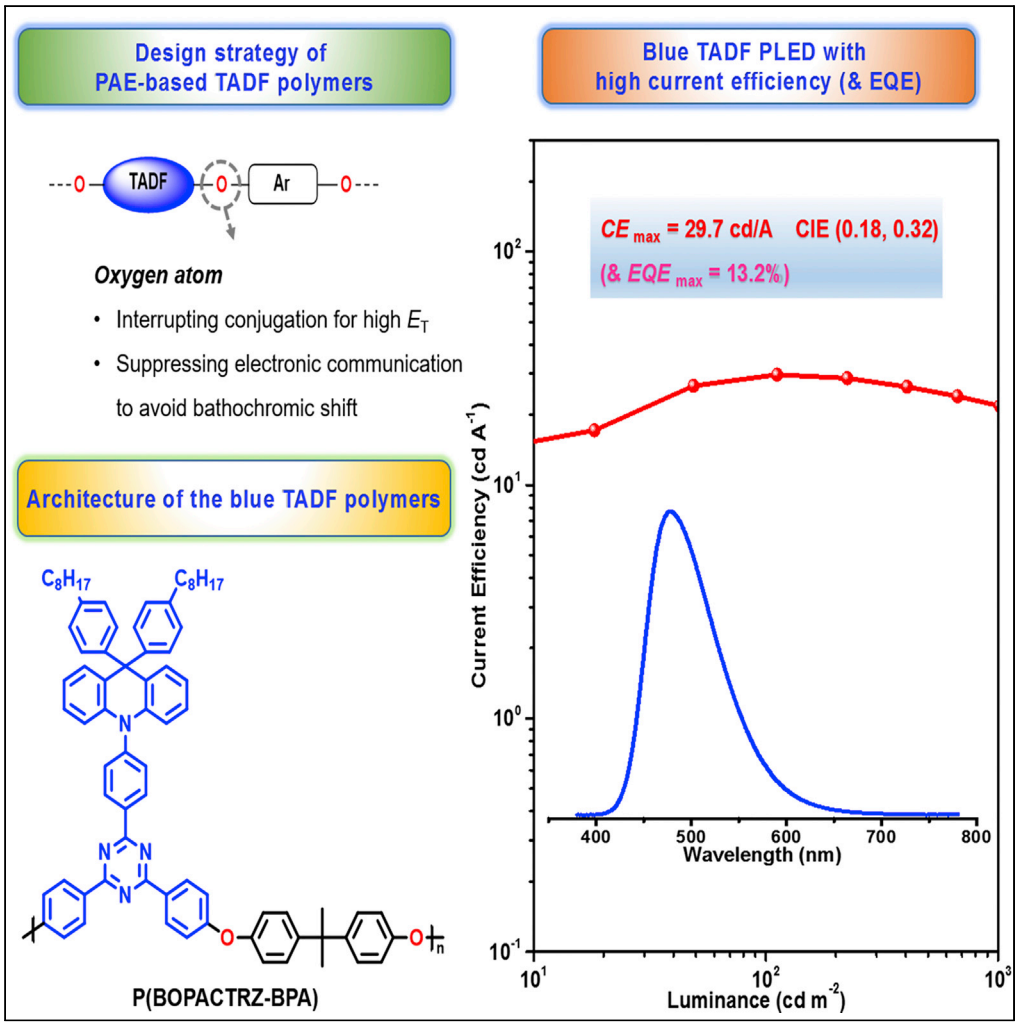


Xinrui Liu, Jiancheng Rao, Xuefei Li, Shumeng Wang, Junqiao Ding, Lixiang Wang

wangshumeng@ciac.ac.cn (S.W.)
junqiaod@ciac.ac.cn (J.D.)

## HIGHLIGHTS

Directly embedding a small molecular blue TADF emitter in a poly(aryl ether) backbone

Oxygen-induced negligible electron communication leads to blue delayed fluorescence

The achieved device efficiency is competitive with blue phosphorescent polymers

Liu et al., iScience *15*, 147–155
May 31, 2019 
https://doi.org/10.1016/j.isci.2019.04.020

iScience

CellPress

Article

# Teaching an Old Poly(arylene ether) New Tricks: Efficient Blue Thermally Activated Delayed Fluorescence

Xinrui Liu,[1,2] Jiancheng Rao,[1,3] Xuefei Li,[1,2] Shumeng Wang,[1,*] Junqiao Ding,[1,2,4,*] and Lixiang Wang[1,2]

## SUMMARY

**Polymer light-emitting diodes are attractive for optoelectronic applications owing to their brightness and ease of processing. However, often metals have to be inserted to increase the luminescence efficiency, and producing blue emitters is a challenge. Here we present a strategy to make blue thermally activated delayed fluorescence (TADF) polymers by directly embedding a small molecular blue TADF emitter into a poly(aryl ether) (PAE) backbone. Thanks to the oxygen-induced negligible electronic communication between neighboring TADF fragments, its corresponding blue delayed fluorescence can be inherited by the developed polymers. These polymers are free from metal catalyst contamination and show improved thermal stability. Through device optimization, a current efficiency of 29.7 cd/A (21.2 lm/W, 13.2%) is realized together with Commission Internationale de L'Eclairage coordinates of (0.18, 0.32). The value is competitive with blue phosphorescent polymers, highlighting the importance of the PAE backbone in achieving high-performance blue delayed fluorescence at a macromolecular level.**

## INTRODUCTION

Polymer light-emitting diodes (PLEDs) fabricated via cost-effective wet methods have attracted much attention because of their potential applications in large-area and flexible flat panel displays and solid-state lightings (Kraft et al., 1998; Grimsdale et al., 2009; Shao et al., 2018). Dating back to the 1990s, the early developed electroluminescent polymers for PLEDs were based on fluorescence (Burroughes et al., 1990), in which only singlet excitons could be utilized to give limited internal quantum efficiency (IQE) below 25% (Segal et al., 2003; Baldo et al., 1999). To harvest both singlet and triplet excitons, phosphorescent polymers containing noble metal complexes were subsequently demonstrated and achieved a near-unity IQE (Xu et al., 2015; Liang et al., 2014). Until recently, thermally activated delayed fluorescent (TADF) polymers have caught the public's eye (Liu et al., 2018; Zou et al., 2018). Without any noble metals, they can realize comparable efficiency to phosphorescent polymers through a rapid reverse intersystem crossing (RISC) from the lowest triplet state ($T_1$) to the lowest singlet state ($S_1$) with the help of the environmental thermal energy (Endo et al., 2009; Uoyama et al., 2012; Zhang et al., 2014). Although great progress has been made in developing green to red TADF polymers nowadays (Nikolaenko et al., 2015; Lee et al., 2016; Ren et al., 2016; Zhu et al., 2016; Freeman et al., 2017; Li et al., 2017; Xie et al., 2017; Yang et al., 2018a, 2018b), there are a few examples of efficient TADF polymers with blue emission (Shao et al., 2017; Zeng et al., 2018).

The challenge lies in the dearth of a polymer backbone with high triplet energy ($E_T$) (van Dijken et al., 2004) because most of the conjugated polymers have too low $E_T$ to prevent the triplet energy back transfer from the TADF unit to the backbone (Sudhakar et al., 2003; Youn Lee et al., 2012). As an alternative, a nonconjugated backbone is adopted for the design of blue TADF polymers. For example, Shao et al. reported a polyethylene pended with suitable electron donor (D) and acceptor (A) units (Figure 1A) (Shao et al., 2017). Benefiting from the through-space charge transfer (TSCT) effect, a bright blue emission was obtained accompanied by a maximum current efficiency of 24.8 cd/A and an external quantum efficiency (EQE) of 12.1%. However, it is not an easy task to delicately control the distance between D and A, for the bulky solubilizing substituents may weaken TSCT and result in poor device performance. Then Zeng et al. developed blue TADF polymers by simply introducing a blue TADF emitter into the side chain of polynorbornene (Figure 1A) (Zeng et al., 2018). Owing to the insulating nature, the corresponding PLEDs showed extremely low current density, leading to an inferior current efficiency of 13.5 cd/A (7.3%). Therefore both a simple and an effective molecular design are highly desirable for blue TADF polymers.

[1]State Key Laboratory of Polymer Physics and Chemistry, Changchun Institute of Applied Chemistry, Chinese Academy of Sciences, Changchun 130022, P. R. China

[2]University of Science and Technology of China, Hefei 230026, P. R. China

[3]University of Chinese Academy of Sciences, Beijing 100049, P. R. China

[4]Lead Contact

*Correspondence: wangshumeng@ciac.ac.cn (S.W.), junqiaod@ciac.ac.cn (J.D.)

https://doi.org/10.1016/j.isci.2019.04.020

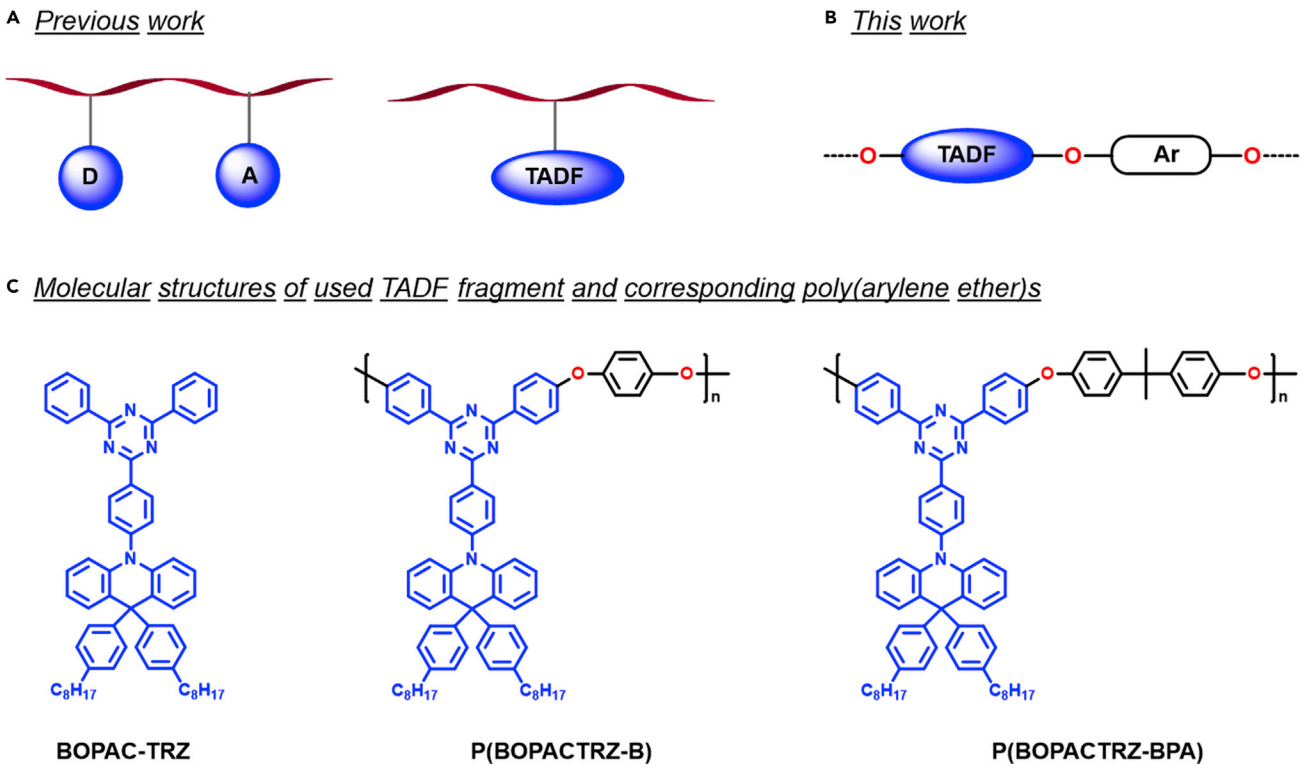


**Figure 1. Schematic Representation of Blue TADF Polymers**

(A) Routes of TADF polymers' molecular design in the literature.

(B) Routes of TADF polymers' molecular design in this work.

(C) Schematic representation of used TADF fragment and corresponding blue TADF polymers in this work.

Also see Scheme S1 and Figures S12–S21.

Herein, we propose a novel strategy to efficient blue TADF from an old poly(arylene ether) (PAE), where a small molecular blue TADF emitter is directly embedded in its backbone. As depicted in Figure 1B, the involved oxygen atom can not only interrupt the conjugation to keep high $E_T$ for the polymer backbone but also suppress the electronic communication between neighboring TADF fragments to avoid the unwanted bathochromic shift. Combined with the freedom of metal catalyst contamination and intrinsic thermal stability, PAE is believed to be a promising platform to realize blue TADF. As a proof of concept, BOPAC-TRZ is selected as the embedded TADF unit (Figure 1C), because its analog DPAC-TRZ without octyl groups possesses efficient blue delayed fluorescence (Lin et al., 2016) and the triazine component has enough nucleophilic aromatic substitution polymerization reactivity (Strukelj and Hedrick, 1994; Yu et al., 2009). With the commercially available comonomer 1,4-dihydroxybenzene or bisphenol A in hand, two blue TADF polymers P(BOPACTRZ-B) and P(BOPACTRZ-BPA) have been successfully constructed based on the PAE backbone. The corresponding devices reveal a record-high current efficiency of 29.7 cd/A (13.2%) as well as Commission Internationale de L'Eclairage (CIE) coordinates of (0.18, 0.32). To the best of our knowledge, the obtained efficiency is the highest value reported so far for blue TADF polymers.

## RESULTS AND DISCUSSION

The monomer and polymer synthesis is presented in Scheme S1. Starting from 2-(phenylamino) benzoic acid, the key intermediate 9,9-bis(4-octylphenyl)-9,10-dihydroacridine (**2**) was first prepared through esterification and subsequent *in situ* cyclization, in which the two octyl groups were introduced to ensure PAE solubility. Then a copper-catalyzed selective C-N coupling between **2** and 1-bromo-4-iodobenzene was performed to give 10-(4-bromophenyl)-9,9-bis(4-octylphenyl)-9,10-dihydroacridine (**3**). After being converted to its corresponding boric acid ester (**4**), the difluorinated blue TADF monomer M1 was produced via a Suzuki-Miyaura reaction in a moderate yield of 52%. For comparison, the small-molecular blue TADF emitter BOPAC-TRZ without fluorine atoms was also synthesized as the reference. Finally, a nucleophilic

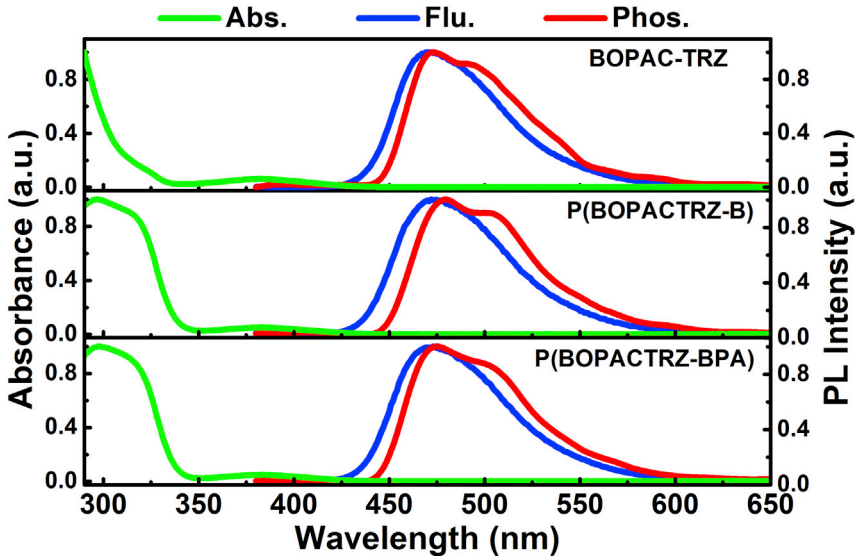


**Figure 2. Ultraviolet-Visible Absorption Spectra in Toluene, Fluorescence and Phosphorescence Spectra in the Neat Films of P(BOPACTRZ-B) and P(BOPACTRZ-BPA) Compared with BOPAC-TRZ**

aromatic substitution polymerization between M1 and 1,4-dihydroxybenzene or bisphenol A was carried out to afford the polymers P(BOPACTRZ-B) and P(BOPACTRZ-BPA) (Johnson et al., 1967; Hale et al., 1967; Johnson and Farnham, 1967). In this case, $K_2CO_3$ instead of palladium was used as the catalyst, thus eliminating the detrimental effect of metal catalyst residue on device performance (Krebs et al., 2004). Moreover, the number-average molecular weight (Mn) and polydispersity index determined by gel permeation chromatography are 10.7 kDa and 1.6 for P(BOPACTRZ-B) and 56.5 kDa and 1.4 for P(BOPACTRZ-BPA). Owing to the introduction of two additional octyl groups in BOPAC-TRZ, they are readily soluble in common organic solvents, such as toluene, chlorobenzene, and tetrahydrofuran (THF). They are also thermally stable with a decomposition temperature ($T_d$) above 410°C and a glass transition temperature ($T_g$) above 150°C (Figure S1). Compared with BOPAC-TRZ ($T_d$ = 360°C, $T_g$ = 50°C), the improved thermal stability clearly suggests the advantage of the PAE backbone.

| Compound | $\lambda_{abs}$[a] (nm) | $\lambda_{em}$[b] (nm) | $\Phi_{PL}$[c] (%) | $\tau_p$[d] (ns) | $\tau_d$[d] (ns) | $E_S/E_T/\Delta E_{ST}$[e] (eV) | $E_g$[f] (eV) | HOMO[g] (eV) | LUMO[g] (eV) | $T_g$[h] (°C) | $T_d$[i] (°C) | Mn (kDa) | PDI |
|---|---|---|---|---|---|---|---|---|---|---|---|---|---|
| BOPAC-TRZ | 290, 381 | 472 | 75.5 | 25.2 | 1,654.4 | 2.82/2.76/ 0.06 | 2.86 | −5.44 | −2.58 | 50 | 360 | – | – |
| P(BOPACTRZ-B) | 296, 382 | 472 | 44.5 | 19.7 | 1,172.4 | 2.83/2.76/ 0.07 | 2.88 | −5.43 | −2.55 | 150 | 436 | 10.7 | 1.6 |
| P(BOPACTRZ-BPA) | 298, 383 | 473 | 75.3 | 21.8 | 1,623.5 | 2.84/2.78/ 0.06 | 2.86 | −5.41 | −2.55 | 167 | 410 | 56.5 | 1.4 |

**Table 1. Physical Properties of P(BOPACTRZ-B) and P(BOPACTRZ-BPA) Compared with BOPAC-TRZ**

Also see Figures S1–S5 and S9, and Table S1.

PDI, polydispersity index.

[a]Measured in toluene at a concentration of $1 \times 10^{-4}$ M.

[b]Measured in neat films.

[c]Measured by integrating sphere in neat films under $N_2$.

[d]The prompt and delayed fluorescence lifetimes detected in neat films under $N_2$ at 298 K.

[e]$\Delta E_{ST} = E_S - E_T$, where $E_S$ and $E_T$ are estimated from the onsets of the fluorescence and phosphorescence spectra, respectively.

[f]Optical band gap estimated from the absorption onset.

[g]HOMO = -e ($E_{onset,\ ox}$ + 4.8 V), LUMO = HOMO + $E_g$, where $E_{onset,\ ox}$ is the onset of the first oxidation wave.

[h]Glass transition temperatures determined by differential scanning calorimetry.

[i]Decomposition temperatures corresponding to a 5% weight loss determined by thermo gravimetric analysis (TGA).

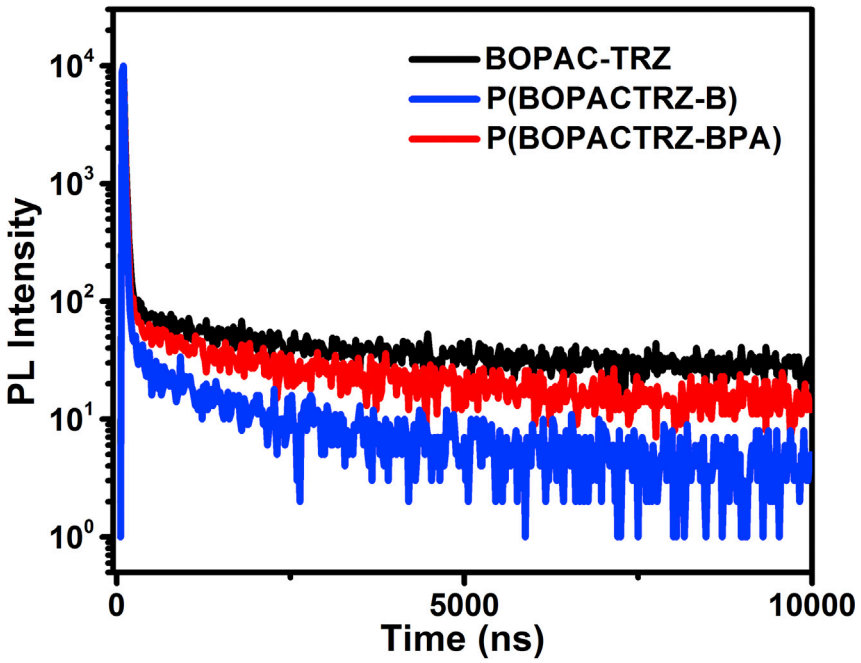


**Figure 3. PL Decay Measured at 298 K under $N_2$ for the Neat Films of P(BOPACTRZ-B) and P(BOPACTRZ-BPA) Compared with BOPAC-TRZ**

Also see Figures S4, S5, and S9, and Table S1.

The highest occupied molecular orbital (HOMO) and lowest unoccupied molecular orbital (LUMO) energy levels of P(BOPACTRZ-B) and P(BOPACTRZ-BPA) are estimated to be −5.41∼-5.43 eV and −2.55 eV, respectively. The values are nearly identical to those of the small molecule BOPAC-TRZ (Figure S2), well consistent with the theoretical simulation (Figure S3). Similar to BOPAC-TRZ, the HOMO of P(BOPACTRZ-B) and P(BOPACTRZ-BPA) distributes on the acridine donor, whereas their LUMO is mainly localized on the triazine acceptor. We note that the direct electron communication between neighboring TADF units is blocked by the oxygen atom in the main chain. This is a key factor to keep the independent blue TADF from BOPAC-TRZ when it is imbedded in the PAE backbone.

Figure 2 compares the ultraviolet-visible absorption spectra in toluene and fluorescence and phosphorescence spectra in films for BOPAC-TRZ, P(BOPACTRZ-B), and P(BOPACTRZ-BPA). They all display a weak lowest energy absorption band in the range of 350–450 nm, which is related to the charge transfer transition from acridine to triazine (Lin et al., 2016). With regard to BOPAC-TRZ, an additional intense absorption around 295–350 nm newly appears in P(BOPACTRZ-B) and P(BOPACTRZ-BPA), indicative of the formation of a PAE backbone (Strukelj and Hedrick, 1994; Yu et al., 2009). Meanwhile, the fluorescence spectra of P(BOPACTRZ-B) and P(BOPACTRZ-BPA) turn out to be the same as that of BOPAC-TRZ, revealing a blue light peak at about 472 nm. The observation can be reasonably ascribed to the oxygen-induced negligible electron communication between neighboring TADF units. This is further verified by the matched phosphorescence among BOPAC-TRZ, P(BOPACTRZ-B), and P(BOPACTRZ-BPA). From the onsets of fluorescence and phosphorescence spectra, their corresponding singlet-triplet energy splitting ($\Delta E_{ST}$) is calculated to be about 0.06 eV (Table 1), small enough to ensure efficient RISC from $T_1$ to $S_1$ followed by delayed fluorescence.

To ascertain their TADF features, subsequently, the transient photoluminescence (PL) spectra of P(BOPACTRZ-B) and P(BOPACTRZ-BPA) were detected. As expected, they possess obvious delayed fluorescence originating from BOPAC-TRZ, which is found to disappear or reduce in the presence of $O_2$ (Figure S4). This is a typical characteristic of TADF emitters as a result of the triplet quenching effect from the ground-state $O_2$ molecules. Going from BOPAC-TRZ to P(BOPACTRZ-B), noticeably, the delayed component is significantly decreased (Figure 3). Also, the related lifetime is down from 1,654.4 ns to 1,172.4 ns (Table 1 and Figure S5). In contrast, P(BOPACTRZ-BPA) shows a close delayed fluorescence to BOPAC-TRZ,

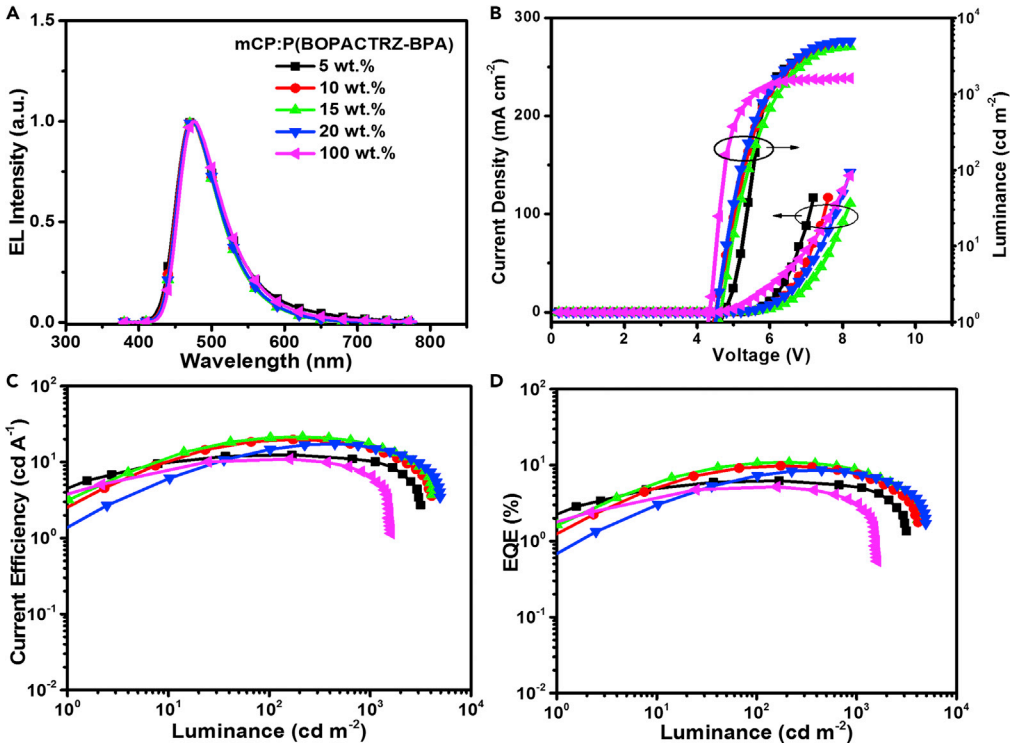


**Figure 4. Device Performance for P(BOPACTRZ-BPA) with PEDOT:PSS as the Hole-Injection Layer**

(A) EL spectra at a driving voltage of 6 V.

(B) Current density-voltage-luminance characteristics.

(C) Current efficiency as a function of luminance.

(D) EQE as a function of luminance.

Also see Figures S6–S10.

giving a lifetime of 1,623.5 ns. Correspondingly, the film PL quantum yield of P(BOPACTRZ-BPA) ($\Phi_{PL}$ = 75.3%) is competent with that of BOPAC-TRZ ($\Phi_{PL}$ = 75.5%), but much higher than that of P(BOPACTRZ-B) ($\Phi_{PL}$ = 44.5%). Supposing the similar influence from the interchain triplet-triplet annihilation (TTA) (Baldo et al., 2000), the intrachain TTA is tentatively responsible for the different TADF behavior for P(BOPACTRZ-B) and P(BOPACTRZ-BPA). As one can see, they only differ from the backbone structure, where BOPAC-TRZ as the blue TADF moiety is separated by 1,4-dihydroxybenzene and bisphenol A, respectively. The distance between neighboring BOPAC-TRZ (denoted as the distance between two triazine rings) is found to increase from 17.5 Å of P(BOPACTRZ-B) to 21.5 Å of P(BOPACTRZ-BPA) (Figure S3). So a much stronger intrachain TTA could be anticipated in P(BOPACTRZ-B), which is well in agreement with its slower RISC rate constant of $T_1$-to-$S_1$ upconversion ($k_{RISC}$) and faster non-radiative rate constant of $T_1$ ($k_{nr}^T$) relative to P(BOPACTRZ-BPA) (Table S1). Further experiments should be carried out to prove this hypothesis, but is beyond the aim of this work.

As discussed above, P(BOPACTRZ-BPA) other than P(BOPACTRZ-B) can well inherit the blue TADF of the small molecule BOPAC-TRZ. Therefore P(BOPACTRZ-BPA) has great potential in electroluminescence (EL). To evaluate this point, PLEDs were assembled with a configuration of ITO/PEDOT: PSS (40 nm)/mCP: P(BOPACTRZ-BPA) (50 nm)/TSPO1 (8 nm)/TmPyPB (42 nm)/LiF (1 nm)/Al (100 nm) (Figure S6). Here PEDOT:PSS (poly(3,4-ethylenedioxythiophene): poly(styrene sulfonate)), mCP (1,3-bis(9H-carbazol-9-yl) benzene), TSPO1 (diphenyl-4-triphenylsilylphenyl-phosphine oxide), and TmPyPB (1,3,5-tri[(3-pyridyl)-phen-3-yl]benzene) act as the hole-injection, host, exciton-blocking, and electron-transporting materials, respectively. P(BOPACTRZ-BPA) is doped into mCP to constitute the emitting layer. The EL spectra, current density-voltage-luminance characteristics, current efficiency, and EQE as a function of luminance are depicted in Figure 4, and the related data are summarized in Table 2. With varied doping concentration, the EL spectra remain nearly unchanged (Figure 4A). All devices emit a bright blue light merely from

| Doping Concentration | $V_{on}$[a] (V) | $L_{max}$ (cd/m$^2$) | $\eta_c$[b] (cd/A) | $\eta_p$[b] (lm/W) | EQE[b] (%) | $\lambda_{em}$ (nm) | CIE (x, y) |
|---|---|---|---|---|---|---|---|
| 5 wt %[c] | 4.8 | 3,159 | 12.5/11.0/10.1 | 7.0/6.0/5.3 | 6.2/5.5/5.1 | 472 | (0.19, 0.28) |
| 10 wt %[c] | 4.6 | 4,133 | 19.6/18.9/15.2 | 11.4/10.6/7.9 | 9.8/9.4/7.6 | 472 | (0.17, 0.27) |
| 15 wt %[c] | 4.6 | 4,147 | 21.4/21.4/17.4 | 12.2/12.0/7.4 | 10.8/10.8/8.7 | 472 | (0.17, 0.27) |
| 20 wt %[c] | 4.6 | 4,926 | 17.4/16.8/15.0 | 9.8/9.8/7.9 | 8.6/8.3/7.4 | 472 | (0.17, 0.27) |
| 100 wt %[c] | 4.4 | 1,607 | 11.0/9.9/6.5 | 7.2/6.2/3.7 | 5.2/4.7/3.1 | 476 | (0.18, 0.30) |
| 15 wt %[d] | 3.6 | 7,270 | 29.7/28.7/21.8 | 21.2/19.6/13.2 | 13.2/12.8/9.7 | 477 | (0.18, 0.32) |

**Table 2. Device Performance for P(BOPACTRZ-BPA)**

Also see Figures S6–S8, S10, and S11, and Tables S2 and S3.

[a]Turn-on voltage at 1 cd/m$^2$.

[b]Data at maximum, 200 cd/m$^2$, and 1,000 cd/m$^2$ for current efficiency ($\eta_c$), power efficiency ($\eta_p$), and EQE, respectively.

[c]Devices with PEDOT:PSS as the hole-injection layer.

[d]Devices with PEDOT:PSS + perfluorinated ionomer (v/v 3:2) as the hole-injection layer.

P(BOPACTRZ-BPA), showing similar Commission Internationale de L'Eclairage (CIE) coordinates of (0.17–0.19, 0.27–0.30).

Despite this, it is found that the current density is distinctly dependent on the doping concentration (Figure 4B). At a low doping concentration, charge trap (Li et al., 2014) plays an important role because the HOMO and LUMO levels of P(BOPACTRZ-BPA) lie between those of mCP (Figure S7). Thereby the current density at the same driving voltage is gradually decreased from 5 to 15 wt %. When the content is further up to 100 wt %, carriers can be injected and transported directly on P(BOPACTRZ-BPA), resulting in reversely enhanced current density. Moreover, the turn-on voltage at 1 cd/m$^2$ is down from 4.8 V to 4.4 V in the absence of the mCP host. The observations imply the good charge-transporting capability of P(BOPACTRZ-BPA), even though the non-conjugated bisphenol A is involved in the backbone. Among these devices, the best performance is achieved at a 15 wt % content (Figures 4C and 4D), revealing a maximum luminance of 4,147 cd/m$^2$, a peak current efficiency of 21.4 cd/A, a peak power efficiency of 12.2 lm/W, and a peak EQE of 10.8%. As the transient PL behaviors of P(BOPACTRZ-BPA) doped into mCP are not obviously influenced by the doping concentration (Figure S9), here the mCP host is used not to alleviate the negative concentration quenching as usual, but to provide a charge trap center (Figure S7) to improve hole-electron recombination possibility and thus device performance.

It should be noted that there is a large hole injection barrier of 0.7 eV between PEDOT:PSS and mCP. To solve this problem, PEDOT:PSS is then modified by a perfluorinated ionomer (see Figure S6). According to the literature (Lee et al., 2007), a work function gradient could be formed via self-organization to favor efficient hole injection. Consequently, the turn-on voltage is greatly reduced from 4.6 to 3.6 V without obviously changing the emission color (CIE: (0.18, 0.32)). The luminance, current efficiency, power efficiency, and EQE are further optimized to be 7,270 cd/m$^2$, 29.7 cd/A, 21.2 lm/W, and 13.2%, respectively (Figure 5). Even at a high luminance of 200 and 1,000 cd/m$^2$, the current efficiency still remains at 28.7 and 21.8 cd/A, respectively, indicative of the small efficiency roll-off. The values are the highest ever reported for blue TADF polymers, and even superior to blue phosphorescent polymers (Table S2), which suggests that the PAE backbone is a promising platform to design efficient blue TADF polymers.

## Limitations of Study

With respect to P(BOPACTRZ-BPA), the control device based on the reference BOPAC-TRZ exhibits nearly the same blue EL with CIE coordinates of (0.18, 0.32) but a lower current efficiency of 20.2 cd/A (15.1 lm/W, 8.9%) (Figure S10 and Table S3). As mentioned above, P(BOPACTRZ-BPA) has a better thermal stability than BOPAC-TRZ, thus leading to the improved device efficiency. Accordingly, because of the unstable acridine moiety and the limited device configuration (Song and Lee, 2017), a comparable short device lifetime is also observed for P(BOPACTRZ-BPA) relative to BOPAC-TRZ (Figure S11 and Table S3). These results mean that the device efficiency, color purity, and lifetime of P(BOPACTRZ-BPA) are mainly determined by BOPAC-TRZ. If a suitable small molecular blue TADF emitter is delicately selected to be embedded into the PAE backbone, high-performance blue TADF polymers, which show comparable efficiency to

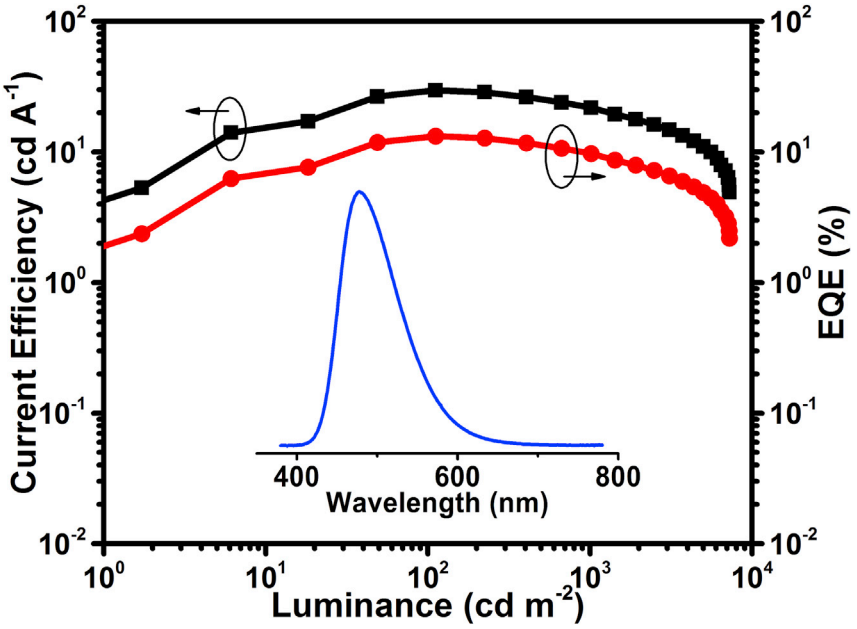


**Figure 5. Current Efficiency and EQE as a Function of Luminance for the Optimized Device of P(BOPACTRZ-BPA) at a Doping Concentration of 15 wt % with PEDOT:PSS + Perfluorinated Ionomer (v/v 3:2) as the Hole-Injection Layer**

Inset: EL spectra at a driving voltage of 6 V. Also see Figures S6, S10, and S11, and Tables S2 and S3.

solution-processible small molecules and dendrimers (Huang et al., 2018), good color purity with a CIE y-coordinate value <0.20 (Sun et al., 2015), as well as longer lifetime toward practical applications, can be further constructed through such a design strategy. And the related work is under way.

## Conclusion

In summary, highly efficient blue TADF polymers have been demonstrated by simply embedding a small molecular TADF emitter into the PAE backbone. They are free of metal catalyst contamination and exhibit improved thermal stability. Also, they are able to inherit the blue delayed fluorescence from the TADF fragment thanks to the oxygen-induced negligible electronic communication. As a result, the corresponding device realizes a state-of-art current efficiency as high as 29.7 cd/A (21.2 lm/W, 13.2%) together with CIE coordinates of (0.18, 0.32). The obtained performance can well compete with that of blue phosphorescent polymers, representing the first example of PAE-based blue TADF polymers. This work, we believe, will open up a new era in PAE used for PLEDs (Shao et al., 2016).

## METHODS

All methods can be found in the accompanying Transparent Methods supplemental file.

## SUPPLEMENTAL INFORMATION

Supplemental Information can be found online at https://doi.org/10.1016/j.isci.2019.04.020.

## ACKNOWLEDGMENTS

The authors acknowledge the National Natural Science Foundation of China (Nos. 51873205, 51573183 and 51703223), the National Key Research and Development Program (2016YFB0401301), and the 973 Project (2015CB655001) for the financial support.

## AUTHOR CONTRIBUTIONS

J.-Q.D. and L.-X.W. coordinated and directed the study. S.-M.W. and J.-Q.D. conceived the idea and designed the experiments. X.-R.L. and J.-C.R. synthesized and characterized the polymers. X.-F.L. fabricated and characterized the devices. X.-R.L., S.-M.W., and J.-Q.D. wrote and revised the manuscript.

## DECLARATION OF INTERESTS

The authors declare no competing interests.

Received: March 12, 2019
Revised: April 10, 2019
Accepted: April 16, 2019
Published: May 31, 2019

## REFERENCES

Baldo, M.A., O'brien, D.F., Thompson, M.E., and Forrest, S.R. (1999). Excitonic singlet-triplet ratio in a semiconducting organic thin film. Phys. Rev. B *60*, 14422–14428.

Baldo, M.A., Adachi, C., and Forrest, S.R. (2000). Transient analysis of organic electrophosphorescence. II. Transient analysis of triplet-triplet annihilation. Phys. Rev. B *62*, 10967.

Burroughes, J.H., Bradley, D.D.C., Brown, A.R., Marks, R.N., Mackay, K., Friend, R.H., Burns, P.L., and Holmes, A.B. (1990). Light-emitting diodes based on conjugated polymers. Nature *347*, 539–541.

van Dijken, A., Bastiaansen, J.J., Kiggen, N.M., Langeveld, B.M., Rothe, C., Monkman, A., Bach, I., Stossel, P., and Brunner, K. (2004). Carbazole compounds as host materials for triplet emitters in organic light-emitting diodes: polymer hosts for high-efficiency light-emitting diodes. J. Am. Chem. Soc. *126*, 7718–7727.

Endo, A., Ogasawara, M., Takahashi, A., Yokoyama, D., Kato, Y., and Adachi, C. (2009). Thermally activated delayed fluorescence from $Sn^{4+}$-porphyrin complexes and their application to organic light-emitting diodes - a novel mechanism for electroluminescence. Adv. Mater. *21*, 4802–4806.

Freeman, D.M.E., Musser, A.J., Frost, J.M., Stern, H.L., Forster, A.K., Fallon, K.J., Rapidis, A.G., Cacialli, F., McCulloch, I., Clarke, T.M., et al. (2017). Synthesis and exciton dynamics of donor-orthogonal acceptor conjugated polymers: reducing the singlet–triplet energy gap. J. Am. Chem. Soc. *139*, 11073–11080.

Grimsdale, A.C., Leok Chan, K., Martin, R.E., Jokisz, P.G., and Holmes, A.B. (2009). Synthesis of light-emitting conjugated polymers for applications in electroluminescent devices. Chem. Rev. *109*, 897–1091.

Hale, W.F., Farnham, A.G., Johnson, R.N., and Clendinning, R.A. (1967). Poly (aryl ethers) by nucleophilic aromatic substitution. II. Thermal stability. J. Polym. Sci. A Polym. Chem. *5*, 2399–2414.

Huang, T., Jiang, W., and Duan, L. (2018). Recent progress in solution processable TADF materials for organic light-emitting diodes. J. Mater. Chem. C *6*, 5577–5596.

Johnson, R.N., and Farnham, A.G. (1967). Poly (aryl ethers) by nucleophilic aromatic substitution. III. Hydrolytic side reactions. J. Polym. Sci. A Polym. Chem. *5*, 2415–2427.

Johnson, R.N., Farnham, A.G., Clendinning, R.A., Hale, W.F., and Merriam, C.N. (1967). Poly (aryl ethers) by nucleophilic aromatic substitution. I. Synthesis and properties. J. Polym. Sci. A Polym. Chem. *5*, 2375–2398.

Kraft, A., Grimsdale, A.C., and Holmes, A.B. (1998). Electroluminescent conjugated polymers-seeing polymers in a new light. Angew. Chem. Int. Ed. *37*, 402–428.

Krebs, F.C., Nyberg, R.B., and Jørgensen, M. (2004). Influence of residual catalyst on the properties of conjugated polyphenylenevinylene materials: palladium nanoparticles and poor electrical performance. Chem. Mater. *16*, 1313–1318.

Lee, T.W., Chung, Y., Kwon, O., and Park, J.J. (2007). Self-organized gradient hole injection to improve the performance of polymer electroluminescent devices. Adv. Funct. Mater. *17*, 390–396.

Lee, S.Y., Yasuda, T., Komiyama, H., Lee, J., and Adachi, C. (2016). Thermally activated delayed fluorescence polymers for efficient solution-processed organic light-emitting diodes. Adv. Mater. *28*, 4019–4024.

Li, H., Li, C., Duan, L., and Qiu, Y. (2014). Charge transport in amorphous organic semiconductors: effects of disorder, carrier density, traps, and scatters. Isr. J. Chem. *54*, 918–926.

Li, C., Nobuyasu, R.S., Wang, Y., Dias, F.B., Ren, Z., Bryce, M.R., and Yan, S. (2017). Solution-processable thermally activated delayed fluorescence white OLEDs based on dual-emission polymers with tunable emission colors and aggregation-enhanced emission properties. Adv. Opt. Mater. *5*, 1700435.

Liang, A., Ying, L., and Huang, F. (2014). Recent progresses of iridium complex-containing macromolecules for solution-processed organic light-emitting diodes. J. Inorg. Organomet. Polym. *24*, 905–926.

Lin, T.-A., Chatterjee, T., Tsai, W.-L., Lee, W.-K., Wu, M.-J., Jiao, M., Pan, K.-C., Yi, C.-L., Chung, C.-L., Wong, K.T., et al. (2016). Sky-blue organic light emitting diode with 37% external quantum efficiency using thermally activated delayed fluorescence from spiroacridine-triazine hybrid. Adv. Mater. *28*, 6976–6983.

Liu, Y., Li, C., Ren, Z., Yan, S., and Bryce, M.R. (2018). All-organic thermally activated delayed fluorescence materials for organic light-emitting diodes. Nat. Rev. Mater. *3*, 18020.

Nikolaenko, A.E., Cass, M., Bourcet, F., Mohamad, D., and Roberts, M. (2015). Thermally activated delayed fluorescence in polymers: a new route toward highly efficient solution processable OLEDs. Adv. Mater. *27*, 7236–7240.

Ren, Z., Nobuyasu, R.S., Dias, F.B., Monkman, A.P., Yan, S., and Bryce, M.R. (2016). Pendant homopolymer and copolymers as solution-processable thermally activated delayed fluorescence materials for organic light-emitting diodes. Macromolecules *49*, 5452–5460.

Segal, M., Baldo, M.A., Holmes, R.J., Forrest, S.R., and Soos, Z.G. (2003). Excitonic singlet-triplet ratios in molecular and polymeric organic materials. Phys. Rev. B *68*, 075211.

Shao, S., Ding, J., and Wang, L. (2016). New applications of poly(arylene ether)s in organic light-emitting diodes. Chin. Chem. Lett. *27*, 1201–1208.

Shao, S., Hu, J., Wang, X., Wang, L., Jing, X., and Wang, F. (2017). Blue thermally activated delayed fluorescence polymers with nonconjugated backbone and through-space charge transfer effect. J. Am. Chem. Soc. *139*, 17739–17742.

Shao, S., Ding, J., and Wang, L. (2018). Research progress on electroluminescent polymers. Acta Polym. Sin. 198–216.

Song, W., and Lee, J.Y. (2017). Degradation mechanism and lifetime improvement strategy for blue phosphorescent organic light-emitting diodes. Adv. Opt. Mater. *5*, 1600901.

Strukelj, M., and Hedrick, J.C. (1994). Synthesis and characterization of novel poly (aryl ether pyridyltriazine) s. Macromolecules *27*, 7511–7521.

Sudhakar, M., Djurovich, P.I., Hogen-Esch, T.E., and Thompson, M.E. (2003). Phosphorescence quenching by conjugated polymers. J. Am. Chem. Soc. *125*, 7796–7797.

Sun, J.W., Baek, J.Y., Kim, K.-H., Moon, C.-K., Lee, J.-H., Kwon, S.K., Kim, Y.-H., and Kim, J.-J. (2015). Thermally activated delayed fluorescence from azasiline based intramolecular charge-transfer emitter (DTPDDA) and a highly efficient blue light emitting diode. Chem. Mater. *27*, 6675–6681.

Uoyama, H., Goushi, K., Shizu, K., Nomura, H., and Adachi, C. (2012). Highly efficient organic light-emitting diodes from delayed fluorescence. Nature *492*, 234–238.

Xie, G., Luo, J., Huang, M., Chen, T., Wu, K., Gong, S., and Yang, C. (2017). Inheriting the characteristics of TADF small molecule by side-chain engineering strategy to enable bluish-green polymers with high PLQYs up to 74% and external quantum efficiency over 16% in light-emitting diodes. Adv. Mater. *29*, 1604223.

Xu, F., Kim, H.U., Kim, J.H., Jung, B.J., Grimsdale, A.C., and Hwang, D.H. (2015). Progress and perspective of iridium-containing

phosphorescent polymers for light-emitting diodes. Prog. Polym. Sci. *47*, 92–121.

Yang, Y., Wang, S., Zhu, Y., Wang, Y., Zhan, H., and Cheng, Y. (2018a). Thermally activated delayed fluorescence conjugated polymers with backbone-donor/pendant-acceptor architecture for nondoped OLEDs with high external quantum efficiency and low roll-off. Adv. Funct. Mater. *28*, 1706916.

Yang, Y., Zhao, L., Wang, S., Ding, J., and Wang, L. (2018b). Red-emitting thermally activated delayed fluorescence polymers with poly(fluorene-co-3,3up to 74yl diphenyl ether) as the backbone. Macromolecules *51*, 9933–9942.

Youn Lee, S., Yasuda, T., Nomura, H., and Adachi, C. (2012). High-efficiency organic light-emitting diodes utilizing thermally activated delayed fluorescence from triazine-based donor–acceptor hybrid molecules. Appl. Phys. Lett. *101*, 093306.

Yu, G., Liu, C., Wang, J., Chu, C., and Jian, X. (2009). Synthesis of phenyl-s-triazine-based copoly(aryl ether)s derived from hydroquinone and resorcinol. Polym. Degrad. Stab. *94*, 2065–2071.

Zeng, X., Luo, J., Zhou, T., Chen, T., Zhou, X., Wu, K., Zou, Y., Xie, G., Gong, S., and Yang, C. (2018). Using ring-opening metathesis polymerization of norbornene to construct thermally activated delayed fluorescence polymers: high-efficiency blue polymer light-emitting diodes. Macromolecules *51*, 1598–1604.

Zhang, Q., Li, B., Huang, S., Nomura, H., Tanaka, H., and Adachi, C. (2014). Efficient blue organic light-emitting diodes employing thermally activated delayed fluorescence. Nat. Photon. *8*, 326–332.

Zhu, Y., Zhang, Y., Yao, B., Wang, Y., Zhang, Z., Zhan, H., Zhang, B., Xie, Z., Wang, Y., and Cheng, Y. (2016). Synthesis and electroluminescence of a conjugated polymer with thermally activated delayed fluorescence. Macromolecules *49*, 4373–4377.

Zou, Y., Gong, S., Xie, G., and Yang, C. (2018). Design strategy for solution-processable thermally activated delayed fluorescence emitters and their applications in organic light-emitting diodes. Adv. Opt. Mater. *6*, 1800568.

**ISCI, Volume *15***

## Supplemental Information

# Teaching an Old Poly(arylene ether) New Tricks: Efficient Blue Thermally Activated Delayed Fluorescence

**Xinrui Liu, Jiancheng Rao, Xuefei Li, Shumeng Wang, Junqiao Ding, and Lixiang Wang**

**Transparent Methods**

**Measurements and Characterization.** $^{1}H$ and $^{13}C$ NMR spectra were recorded by a Bruker Avance NMR spectrometer. MALDI-TOF mass spectra were recorded on an AXIMA CFR MS apparatus (COMPACT). Elemental analysis was performed using a Bio-Rad elemental analysis system. GPC was carried out on Waters 410 with polystyrene as the standard and THF as the eluent. Thermal gravimetric analysis (TGA) were performed with a PerkinElmer-TGA 7 under nitrogen at a heating rate of 20 $^{o}$C/min. Differential scanning calorimetry (DSC) were recorded on a PerkinElmer-DSC 7 under nitrogen at a heating rate of 10 $^{o}$C/min. UV-visible absorption and PL spectra were performed on a PerkinElmer Lambda 35 UV-vis spectrometer and a PerkinElmer LS 50B spectrofluorometer, respectively. PLQYs were measured using an integrating sphere integrated to HORIBA FL3C-111. Transient PL spectra were detected on an Edinburgh fluorescence spectrometer (FLS-980). Cyclic voltammetry (CV) were performed on EG&G 283 (Princeton Applied Research) potentiostat/galvanostat system. Ferrocene/ferrocenium (Fc/Fc+) and n-$Bu_4NClO_4$ were used as the reference and the supporting electrolyte, respectively. The HOMO and LUMO levels were calculated according to the equations HOMO = -e ($E_{onset,\ ox}$ + 4.8 V), LUMO = HOMO + $E_g$, where $E_{onset,\ ox}$ is the onset value of the first oxidation wave and $E_g$ is the optical bandgap estimated from the absorption onset. Theoretical calculations were carried out using the Gaussian 09 program package. All ground state structures in the gas phase were optimized with density functional theory (DFT) at the M062X/6-311G** level.

**Device fabrication and testing.** The device configuration is ITO/PEDOT:PSS (40 nm)/mCP: P(BOPACTRZ-BPA) (50 nm)/TSPO1 (8 nm)/TmPyPB (42 nm)/LiF (1 nm)/Al

(100 nm). Firstly, the pre-cleaned ITO-coated glass substrates (15 Ω per square) were treated with ultraviolet-ozone for 40 min. Subsequently, the PEDOT:PSS (Bayron P VP AI4083) layer was deposited onto the substrates in air at a speed of 5000 rpm for 40 s, annealed at 120 $^{o}$C for 1 h, and moved into a glove box filled with nitrogen. Then the mixed chlorobenzene solution of mCP and P(BOPACTRZ-BPA) was deposited onto the PEDOT:PSS layer via spin-coating at a speed of 1800 rpm for 60 s to form the emissive layer. After transferred into a vacuum chamber, other layers including 8 nm TSPO1, 42 nm TmPyPB, 1 nm LiF and 100 nm Al were successively evaporated under a base pressure (< 4 × $10^{-4}$ Pa). The current density-voltage-luminance characteristics were tested using a Keithley source measurement unit (Keithley 2400 and Keithley 2000) calibrated with a silicon photodiode. The EL spectra and CIE coordinates were measured on a CS2000 spectra colorimeter. EQE were calculated from the EL spectrum, luminance, and current density, assuming a Lambertian emission distribution. All the measurements were performed at room temperature under ambient atmosphere. To further optimize the device performance, PFI (Nafion® D-521 dispersion, 5% w/w in water and 1-propanol, ≥ 0.92 meq/g exchange capacity, Alfa Aesar) was blended into PEDOT:PSS with a volume ratio of 2:3, and utilized as the hole injection layer instead of PEDOT:PSS.

## Supplemental Schemes

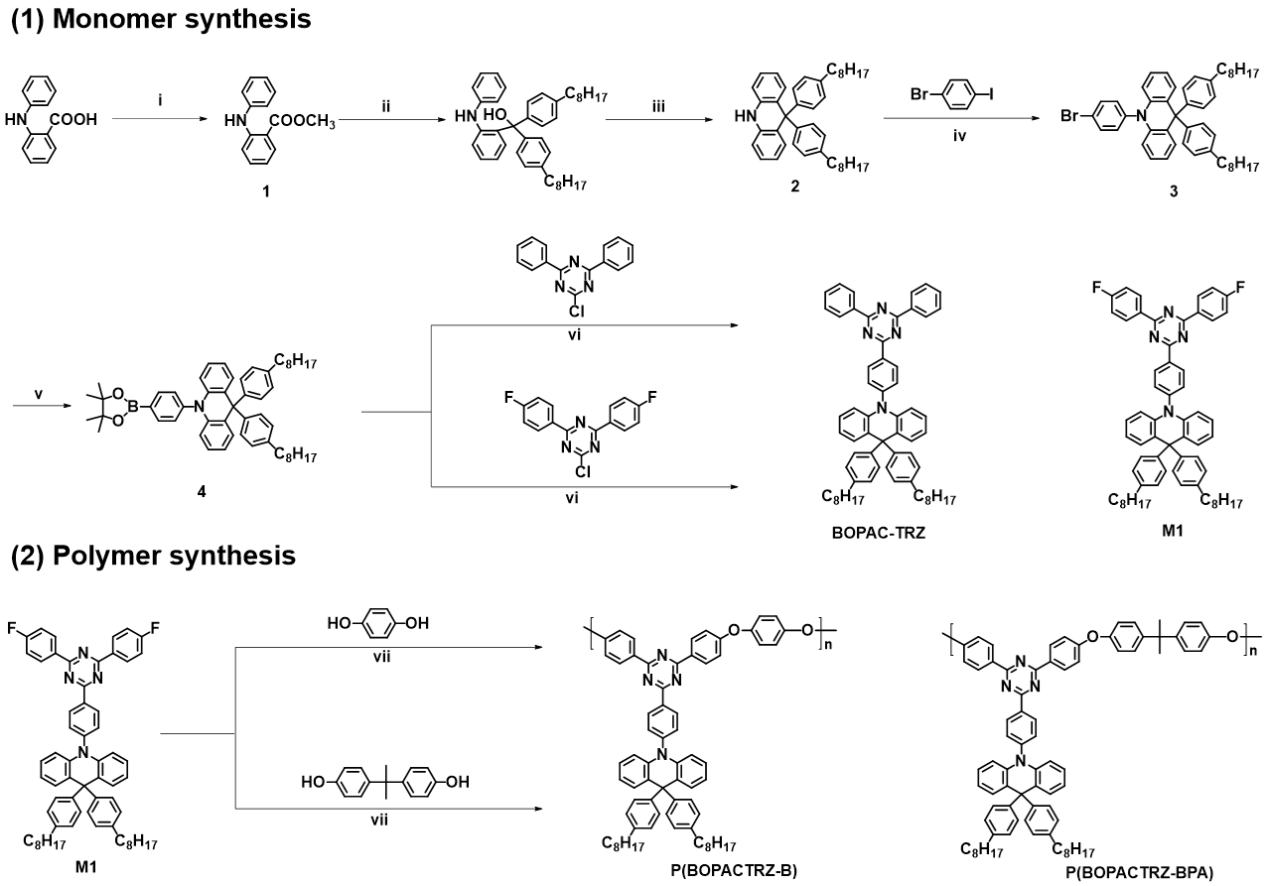


**Scheme S1. Synthetic pathway of the monomer and corresponding blue TADF polymers.** Reagents and conditions: (i) thionyl chloride, MeOH, 60 °C; (ii) 1-bromo-4-octylbenzene, Mg, $I_2$, THF, room temperature; (iii) column chromatography with acid silica-gel; (iv) CuI, t-BuONa, S-DACH, 1,4-dioxane, reflux; (v) bis(pinacolato)diboron, Pd(dppf)$Cl_2$, KOAc, DMF, 80 °C; (vi) $K_2CO_3$ aqueous solution (2 mol/L), Pd($PPh_3$)$_2Cl_2$, toluene, 105 °C; (vii) $K_2CO_3$, toluene/DMAC (*v*/*v* 3:2), 170 °C. Related to Figure 1.

## Synthesis

All raw materials including solvents were purchased from commercial channels, and used directly without further purification unless specifically pointed out. THF and toluene were dried by sodium, and 1,4-dioxane, N,N-dimethylformamide (DMF) and N,N-dimethylacetamide (DMAc) were dried by calcium hydride in advance. 1,4-dihydroxybenzene and bisphenol A were recrystallized from ethanol before

polymerization. The intermediate 2-chloro-4,6-bis(4-fluorophenyl)-1,3,5-triazine were prepared according to the literature (WO Patent 2012110182. 2012-08-23).

*methyl 2-(phenylamino) benzoate* (**1**): 2-(phenylamino) benzoic acid (108.61 g, 0.50 mol) was dissolved in methanol (300 mL) in a 1000 mL three-neck round-bottom flask, followed by a cautious and dropwise addition of thionyl chloride (76 mL). The reaction mixture was stirred at 60 $^{o}$C for 12 h. Then the saturated sodium bicarbonate aqueous solution was added when cooled to room temperature. The organic phase was extracted with dichloromethane, and dried with sodium sulphate anhydrous. After the solvent removal by a rotary vacuum evaporator, the residue was purified by silica-gel column chromatography, with petroleum ether/dichloromethane (*v/v* 5:1) as the eluent, to give a yellow solid **1** (110.00 g, 95%). $^{1}$H NMR (400 MHz, $d_6$-DMSO, δ ppm): 9.32 (s, 1H), 7.90 (d, *J* = 8.0 Hz, 1H), 7.47 – 7.32 (m, 3H), 7.24 (t, *J* = 7.7 Hz, 3H), 7.09 (t, *J* = 7.2 Hz, 1H), 6.81 (t, *J* = 7.5 Hz, 1H), 3.86 (s, 3H).

*9,9-bis(4-octylphenyl)-9,10-dihydroacridine* (**2**): Dry THF (150 mL) was added into a container containing 1-bromo-4-octylbenzene (75.64 g, 0.30 mol). After degassed, the solution was added dropwisely into a two-neck round-bottom flask containing magnesium chips (13.72 g, 0.60 mol), and two grains of iodine at room temperature. The mixture was stirred at 60 $^{o}$C for half an hour, and then transferred to a solution of methyl 2-(phenylamino) benzoate (**1**) (16.03 g, 0.10 mol) in dry THF (50 mL). The mixture was further stirred at room temperature for 12 h, followed by the removal of THF. The residue was dissolved in dichloromethane, washed with saturated sodium chloride aqueous solution, and dried with sodium sulphate anhydrous. After the solvent removal by a rotary vacuum evaporator, the residue was purified by silica-gel column chromatography, with

petroleum ether/dichloromethane (*v/v* 10:1) as the eluent, to give a white solid **2** (32.27 g, 82%). It should be noted that the in-situ cyclization happens during the column chromatography because of the acidity of the used silica-gel. $^1$H NMR (400 MHz, $d_6$-DMSO, δ ppm): 7.15 (s, 2H), 7.01 (d, *J* = 8.2 Hz, 4H), 6.89 – 6.72 (m, 10H), 2.58 – 2.52 (m, 4H), 1.63 – 1.54 (m, 4H), 1.33 – 1.22 (m, 20H), 0.88 (t, *J* = 6.9 Hz, 6H).

*10-(4-bromophenyl)-9,9-bis(4-octylphenyl)-9,10-dihydroacridine* (**3**): 9,9-bis(4-octylphenyl)-9,10-dihydroacridine (**2**) (40.00 g, 71.70 mmol), 1-bromo-4-iodobenzene (30.43 g, 107.60 mmol), CuI (0.27 g, 1.40 mmol), t-BuONa (13.78 g, 0.10 mol), (1S,2S)-(+)-1,2-diaminocyclohexane (S-DACH) (0.82 g, 7.20 mmol) were added into 250 mL 1,4-dioxane. The mixture was stirred under refluxing for 24 h, and extracted with dichloromethane when cooled to room temperature. The organic phase was washed with saturated sodium chloride aqueous solution, and dried with sodium sulphate anhydrous. After the solvent removal by a rotary vacuum evaporator, the residue was purified by silica-gel column chromatography, with petroleum ether as the eluent, to give a colorless, oil-like and viscous matter **2** (45.49 g, 89%). $^1$H NMR (400 MHz, $CDCl_3$, δ ppm): 7.67 (d, *J* = 7.3 Hz, 2H), 7.12 – 6.85 (m, 16H), 6.42 (d, *J* = 7.2 Hz, 2H), 2.74 – 2.50 (m, 4H), 1.63 (s, 4H), 1.32 (m, 20H), 0.92 (s, 6H).

*9,9-bis(4-octylphenyl)-10-(4-(4,4,5,5-tetramethyl-1,3,2-dioxaborolan-2-yl)phenyl)-9,10-dihydroacridine* (**4**): 10-(4-bromophenyl)-9,9-bis(4-octylphenyl)-9,10-dihydroacridine (**3**) (45.48 g, 63.80 mmol), bis(pinacolato)diboron (19.44 g, 76.60 mmol), [1,1'-bis(diphenylphosphino)ferrocene]dichloropalladium(II) ($Pd(dppf)Cl_2$) (2.80 g, 3.80 mmol), and KOAc (37.57 g, 0.40 mol) were added to 250 mL DMF. The mixture was stirred at 80 $^o$C overnight, and poured into water when cooled to room temperature. The

precipitate was collected by filtration, dissolved in dichloromethane, washed with saturated sodium chloride aqueous solution, and dried over sodium sulphate anhydrous. After the solvent removal by a rotary vacuum evaporator, the residue was purified by silica-gel column chromatography, with petroleum ether/ethyl acetate (*v/v* 12:1) as the eluent, to give a white solid **4** (40.73 g, 84%). $^{1}$H NMR (400 MHz, $CDCl_3$, δ ppm): 7.95 (d, *J* = 8.0 Hz, 2H), 7.14 – 6.95 (m, 8H), 6.93 – 6.80 (m, 8H), 6.38 (d, *J* = 8.1 Hz, 2H), 2.68 – 2.50 (m, 4H), 1.76 – 1.50 (m, 6H), 1.37 (s, 10H), 1.29 (m, 20H), 0.88 (t, *J* = 6.8 Hz, 6H).

*10-(4-(4,6-diphenyl-1,3,5-triazin-2-yl)phenyl)-9,9-bis(4-octylphenyl)-9,10-dihydroacridine* (**BOPAC-TRZ**): Toluene (120 mL) and 2 mol/L aqueous $K_2CO_3$ (11.5 mL) were added to a mixture of 2-chloro-4,6-diphenyl-1,3,5-triazine (3.39 g, 12.70 mmol), 9,9-bis(4-octylphenyl)-10-(4-(4,4,5,5-tetramethyl-1,3,2-dioxaborolan-2-yl)phenyl)-9,10-dihydroacridine (**4**) (8.75 g, 11.50 mmol) and bis(triphenylphosphine)palladium(II) chloride ($Pd(PPh_3)_2Cl_2$) (0.28 g, 0.40 mmol). The mixture was heated to 105 °C for 12 h, cooled to room temperature, extracted with dichloromethane and dried over anhydrous sodium sulphate. The solvent was removed under reduced pressure, and the residue was purified by column chromatography on silica gel using petroleum ether/dichloromethane (*v/v* 15:1) as the eluent. Finally, a recrystallization was performed in petroleum ether/dichloromethane (*v/v* 1:1) to produce a yellowish solid **BOPAC-TRZ** (4.38 g, 44%). $^{1}$H NMR (400 MHz, $CDCl_3$, δ ppm): 8.91 (d, *J* = 8.3 Hz, 2H), 8.79 (d, *J* = 7.3 Hz, 4H), 7.71 – 7.54 (m, 6H), 7.29 (d, *J* = 8.3 Hz, 2H), 7.06 (m, 6H), 6.99 – 6.86 (m, 8H), 6.52 (d, *J* = 8.2 Hz, 2H), 2.67 – 2.55 (m, 4H), 1.66 – 1.60 (m, 4H), 1.29 (m, 20H), 0.86 (d, *J* = 6.9 Hz, 6H). $^{13}$C NMR (126 MHz, $CDCl_3$, δ ppm): 171.79, 171.07, 145.03, 143.69, 141.88, 140.77, 136.08, 135.95, 132.65, 131.42, 131.16, 130.34, 130.21, 130.08, 128.99, 128.69, 127.61, 126.74, 120.36, 114.14, 56.20, 35.51, 31.89, 31.39, 29.50, 29.42, 29.29, 22.69, 14.13.

MALDI-TOF (*m/z*) calcd for $C_{62}H_{64}N_4$ $[M + H]^+$: 865.5; Found: 865.5. Anal. Calcd. for $C_{62}H_{64}N_4$: C, 86.07; H, 7.46; N, 6.48; Found: C, 86.08; H, 7.52; N, 6.35.

*10-(4-(4,6-bis(4-fluorophenyl)-1,3,5-triazin-2-yl)phenyl)-9,9-bis(4-octylphenyl)-9,10-dihydroacridine* (**M1**): Toluene (109 mL) and 2 mol/L aqueous $K_2CO_3$ (24 mL) were added to a mixture of 2-chloro-4,6-bis(4-fluorophenyl)-1,3,5-triazine (6.63 g, 21.80 mmol), 9,9-bis(4-octylphenyl)-10-(4-(4,4,5,5-tetramethyl-1,3,2-dioxaborolan-2-yl)phenyl)-9,10-dihydroacridine (**4**) (18.25 g, 24.00 mmol) and bis(triphenylphosphine)palladium(II) chloride ($Pd(PPh_3)_2Cl_2$) (0.46 g, 0.70 mmol). The mixture was heated to 105 ºC for 12 h, cooled to room temperature, extracted with dichloromethane, and dried over anhydrous sodium sulphate. The solvent was removed under reduced pressure, and the residue was purified by column chromatography on silica gel using petroleum ether/dichloromethane (*v/v* 12:1) as the eluent. Finally, a recrystallization was performed in petroleum ether/dichloromethane (*v/v* 1:1) to produce a green solid **M1** (10.23 g, 52%). $^1$H NMR (400 MHz, $CDCl_3$, δ ppm): 8.87 (d, *J* = 8.3 Hz, 2H), 8.78 (dd, *J* = 8.6, 5.6 Hz, 4H), 7.31 – 7.27 (m, 4H), 7.23 – 7.03 (m, 8H), 6.96 – 6.88 (m, 8H), 6.52 (d, *J* = 8.1 Hz, 2H), 2.61 (t, *J* = 7.7 Hz, 4H), 1.63 (m, 4H), 1.30 (m, 20H), 0.88 (t, *J* = 6.7 Hz, 6H). $^{13}$C NMR (126 MHz, $CDCl_3$, δ ppm): 171.07, 170.79, 166.94, 164.92, 145.23, 143.65, 141.85, 140.79, 135.63, 132.14, 132.12, 131.39, 131.37, 131.29, 131.12, 130.45, 130.21, 130.11, 127.61, 126.73, 120.43, 115.89, 115.72, 114.16, 56.22, 35.51, 31.90, 31.39, 22.69, 14.13. MALDI-TOF (*m/z*) calcd for $C_{62}H_{62}F_2N_4$ $[M]^+$: 900.5; Found: 900.5.

*General polymerization procedure*: The polymerization was performed according to a general procedure of PAE. Fluorine-containing monomer (1 equiv.), bisphenol monomer (1 equiv.), toluene/DMAc (*v/v* 3:2, substrate concentration ~ 0.2 mmol/mL) and anhydrous

$K_2CO_3$ (2.4 equiv.) were added in a two-necked glass reactor equipped with a Dean-Stark trap. The mixture was heated to 120 °C for 3 h, and then 150 °C until the toluene was all condensed in the Dean-Stark trap. The reaction temperature was further raised to 170 °C for extra 24 h. 0.05 mmol/mL DMAc solution of fluorine-containing end-blocking agent (0.1 equiv.) and hydroxyl-containing end-blocking agent (0.2 equiv.) were added and retained at 170 °C for 8 h successively. After cooled to room temperature, the mixture was diluted with chloroform. The organic portion was washed with saturated sodium chloride aqueous solution, dried with anhydrous sodium sulphate, and concentrated. The polymer was precipitated with n-hexane, followed by purification with Soxhlet extraction with acetone and methanol, respectively.

**P(BOPACTRZ-B)**: light-yellow powder (0.30 g, 61.6%). **M1** (450.50 mg, 0.50 mmol), 1,4-dihydroxybenzene (55.00 mg, 0.50 mmol), phenol (4.70 mg, 0.05 mmol) and 2-(4-fluorophenyl)-4,6-diphenyl-1,3,5-triazine (32.70 mg, 0.10 mmol) were used in the polymerization. $^1$H NMR (500 MHz, $CDCl_3$, δ ppm): 8.86 (d, *J* = 7.9 Hz, 2H), 8.75 (d, *J* = 8.6 Hz, 4H), 7.28 (d, *J* = 7.7 Hz, 2H), 7.16 (s, 8H), 7.05 (d, *J* = 5.9 Hz, 6H), 6.91 (m, 8H), 6.50 (d, *J* = 8.3 Hz, 2H), 2.58 (s, 4H), 1.61 (s, 4H), 1.34 – 1.22 (m, 20H), 0.86 (d, *J* = 2.9 Hz, 6H). $^{13}$C NMR (126 MHz, $CDCl_3$, δ ppm): 170.99, 170.84, 161.78, 152.26, 144.99, 143.68, 141.87, 140.75, 135.99, 131.39, 131.07, 131.01, 130.74, 130.33, 130.20, 130.10, 129.98, 127.60, 126.72, 121.46, 120.37, 119.90, 117.65, 114.11, 56.19, 35.49, 31.88, 31.37, 29.49, 29.40, 29.28, 22.68, 14.13. Anal. Calcd. for $(C_{68}H_{67}N_4O_2)_n$: C, 84.00; H, 6.95; N, 5.76; Found: C, 84.03; H, 6.95; N, 5.64.

**P(BOPACTRZ-BPA)**: light-yellow fiber (0.56 g, 64.1%). **M1** (703.20 mg, 0.80 mmol), bisphenol A (182.60 mg, 0.80 mmol), 4-(2-phenylpropan-2-yl)phenol (17.00 mg, 0.08 mmol), and 2-(4-fluorophenyl)-4,6-diphenyl-1, 3,5-triazine (52.4 mg, 0.16 mmol) were

used in the polymerization. $^{1}$H NMR (500 MHz, $CDCl_3$, δ ppm): 8.84 (d, *J* = 8.4 Hz, 2H), 8.72 (d, *J* = 8.8 Hz, 4H), 7.27 (d, *J* = 8.6 Hz, 4H), 7.25 – 7.09 (m, 6H), 7.06 – 6.99 (m, 10H), 6.93 – 6.84 (m, 8H), 6.48 (d, *J* = 8.2 Hz, 2H), 2.58 (t, *J* = 7.6 Hz, 4H), 1.71 (d, *J* = 9.7 Hz, 6H), 1.60 (dd, *J* = 14.2, 7.0 Hz, 4H), 1.33 – 1.24 (m, 20H), 0.85 (t, *J* = 6.8 Hz, 6H). $^{13}$C NMR (126 MHz, $CDCl_3$, δ ppm): 171.00, 170.76, 161.76, 153.81, 146.53, 144.91, 143.69, 141.86, 140.74, 136.03, 131.36, 131.06, 130.91, 130.53, 130.26, 130.19, 130.08, 128.28, 127.59, 126.71, 120.34, 119.38, 117.83, 114.10, 56.18, 42.35, 35.49, 31.88, 31.36, 31.06, 29.48, 29.39, 29.27, 22.67, 14.13. Anal. Calcd. for $(C_{77}H_{77}N_4O_2)_n$: C, 84.73; H, 7.20; N, 5.13; Found: C, 84.70; H, 7.14; N, 5.00.

## Supplemental Figures

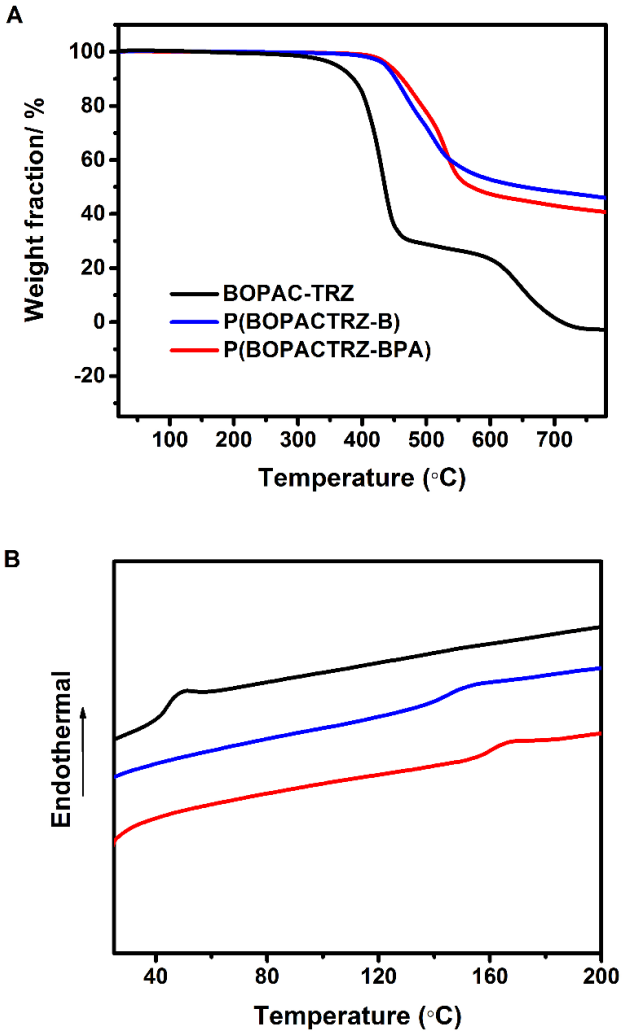


**Figure S1. TGA (A) and DSC traces (B) for P(BOPACTRZ-B) and P(BOPACTRZ-BPA) compared with BOPAC-TRZ.** Related to Table 1.

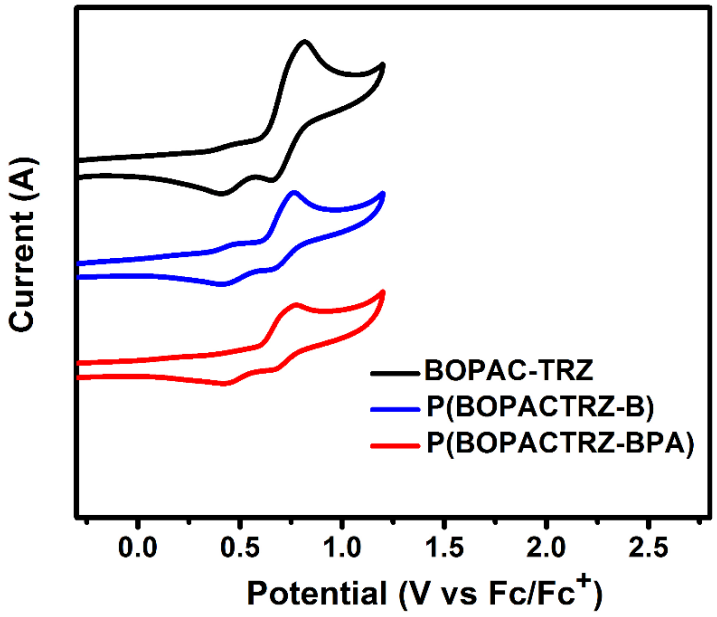


**Figure S2. CV curves recorded in dichloromethane for P(BOPACTRZ-B) and P(BOPACTRZ-BPA) compared with BOPAC-TRZ.** Related to Table 1.

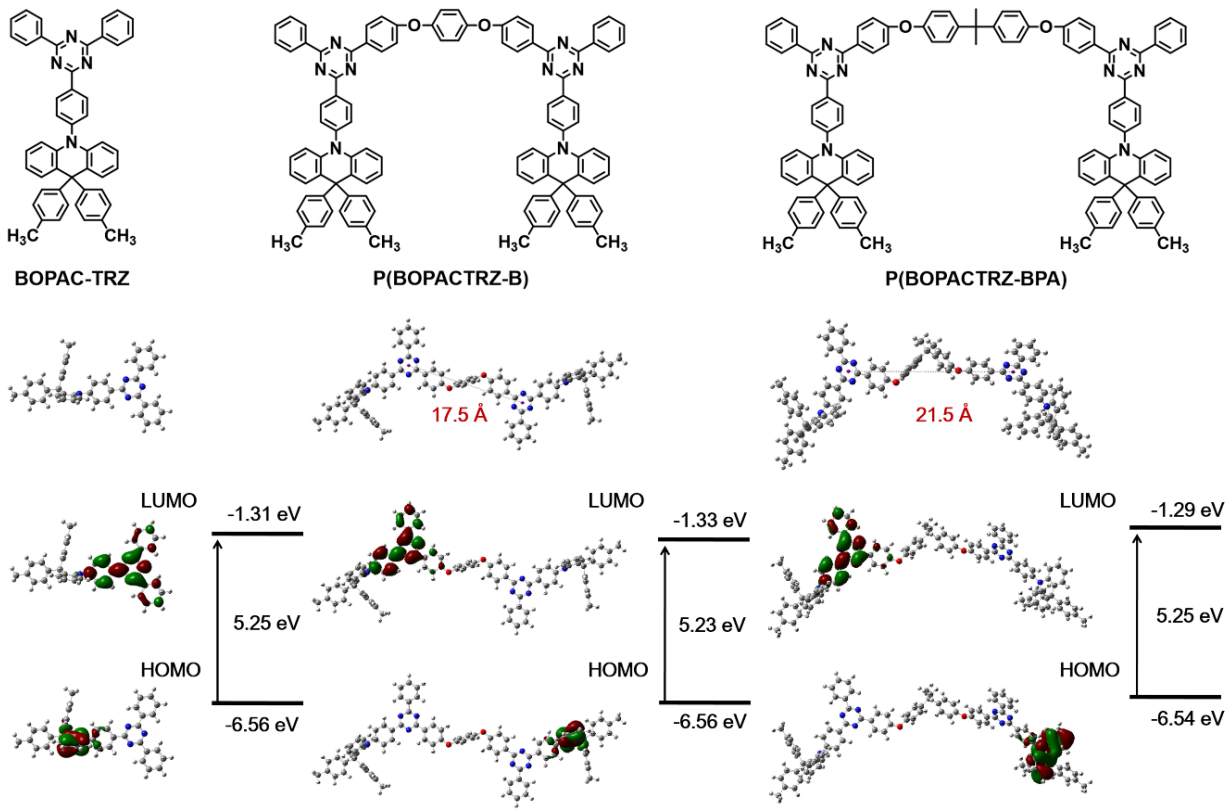


**Figure S3. Simplified molecular structures, optimized geometries and frontier molecular orbital distributions (from top to bottom) for BOPAC-TRZ, P(BOPACTRZ-B) and P(BOPACTRZ-BPA) characterized by DFT calculations [M062X; 6-311G**].** As pointed out, the distance between two triazine rings approximately represents the distance between neighboring TADF units in the PAE. Related to Table 1.

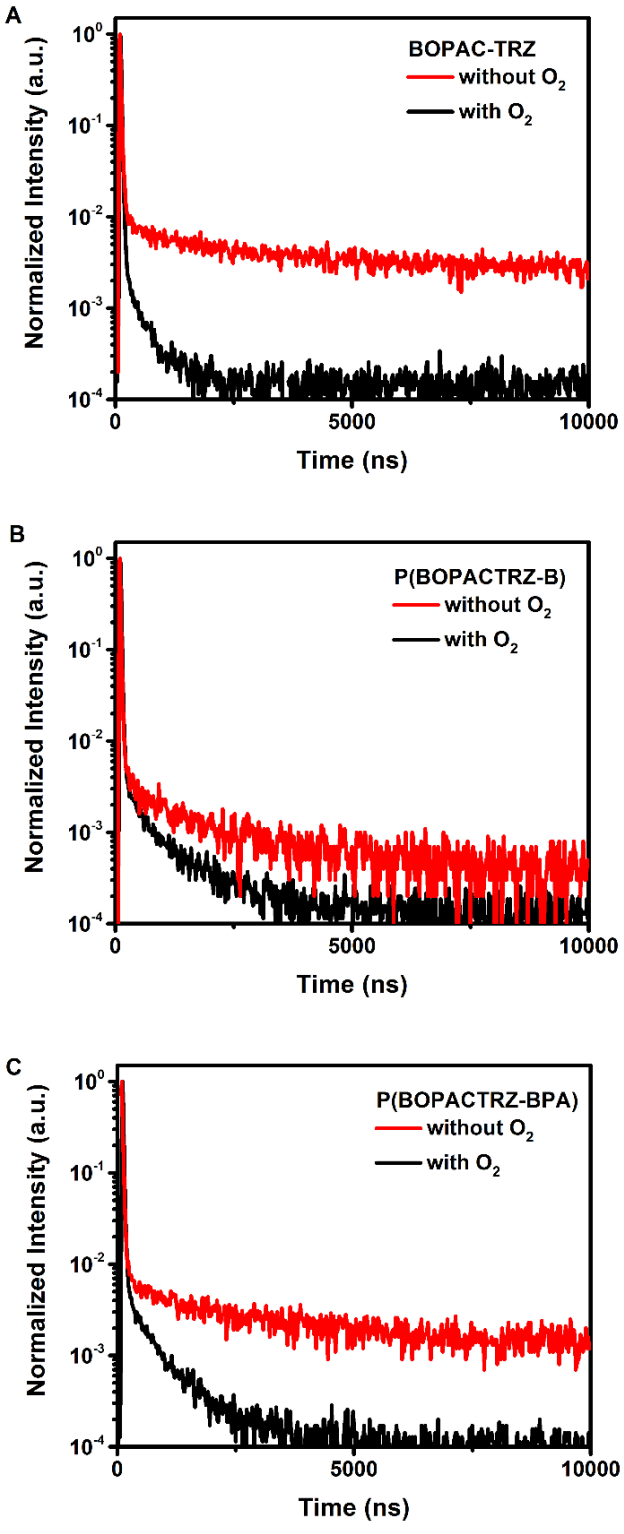


**Figure S4. PL decay measured at 298 K without and with $O_2$ for the neat films**: BOPAC-TRZ (**A**), P(BOPACTRZ-B) (**B**) and P(BOPACTRZ-BPA) (**C**). Related to Figure 3 and Table 1.

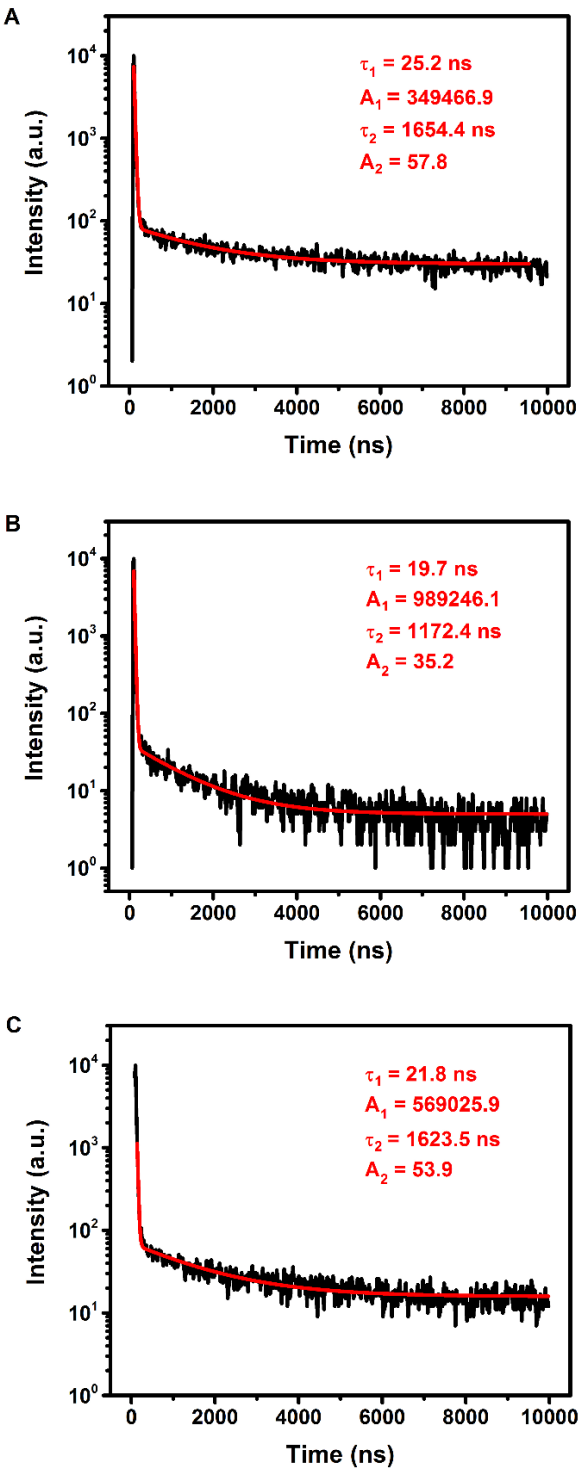


**Figure S5. Transient PL spectra in the absence of $O_2$ as well as the corresponding biexponential fitting results for the neat films**: BOPAC-TRZ (**A**), P(BOPACTRZ-B) (**B**) and P(BOPACTRZ-BPA) (**C**). Related to Figure 3 and Table 1.

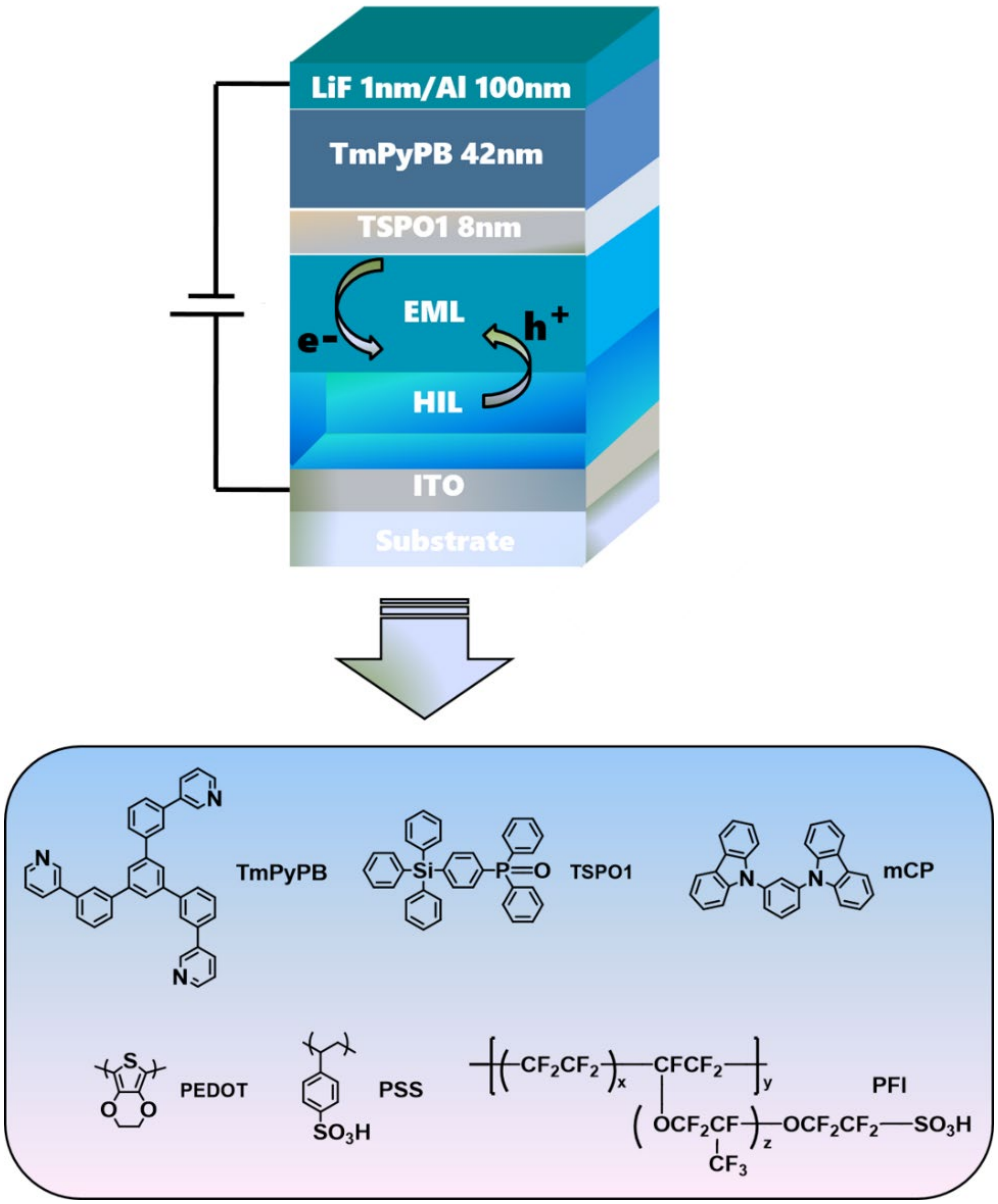


**Figure S6. Device structure and the used chemical structures of functional materials.** Related to Figure 4-5, and Table 2.

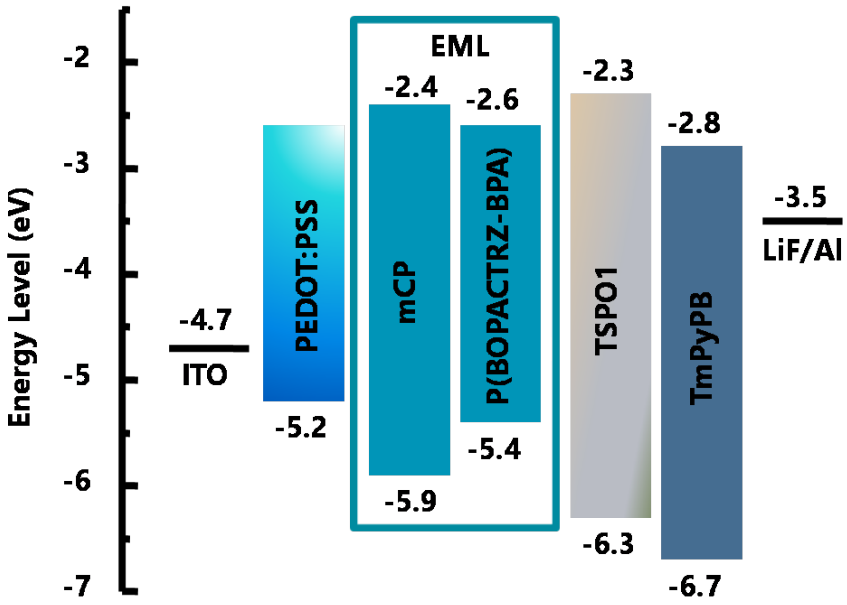


**Figure S7. Energy level alignment for devices of P(BOPACTRZ-BPA) with PEDOT:PSS as the hole-injection layer.** Related to Figure 4 and Table 2.

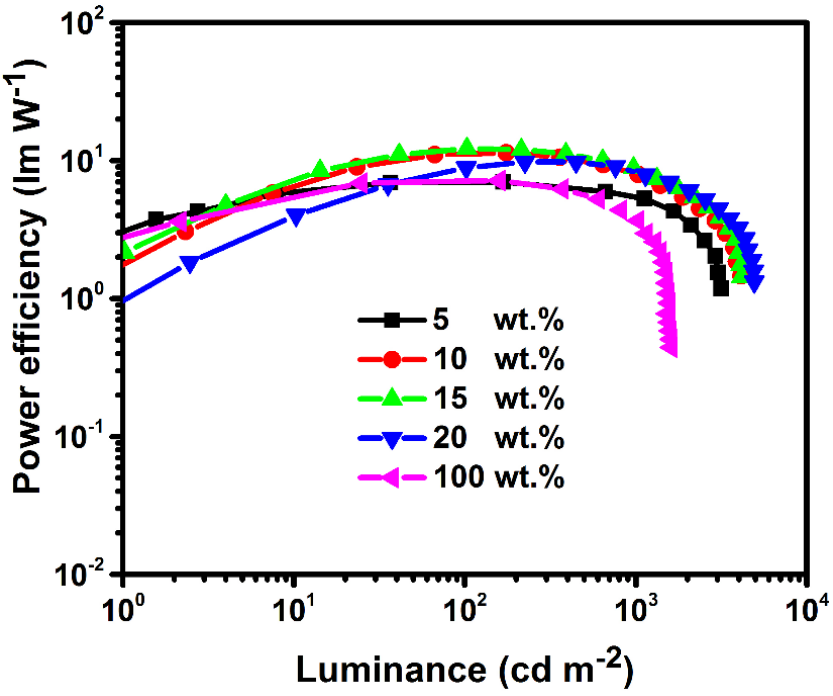


**Figure S8. Power efficiency as a function of luminance for devices of P(BOPACTRZ-BPA) with PEDOT:PSS as the hole-injection layer.** Related to Figure 4 and Table 2.

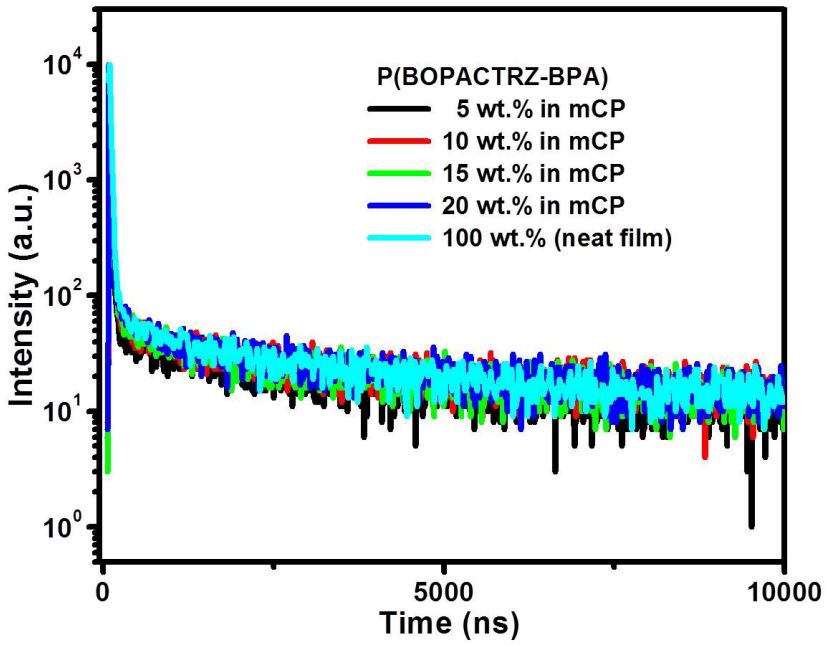


**Figure S9. PL decay curves for mCP:P(BOPACTRZ-BPA) films with different doping concentration measured at 298 K under Ar.** Related to Figure 3 and Table 1.

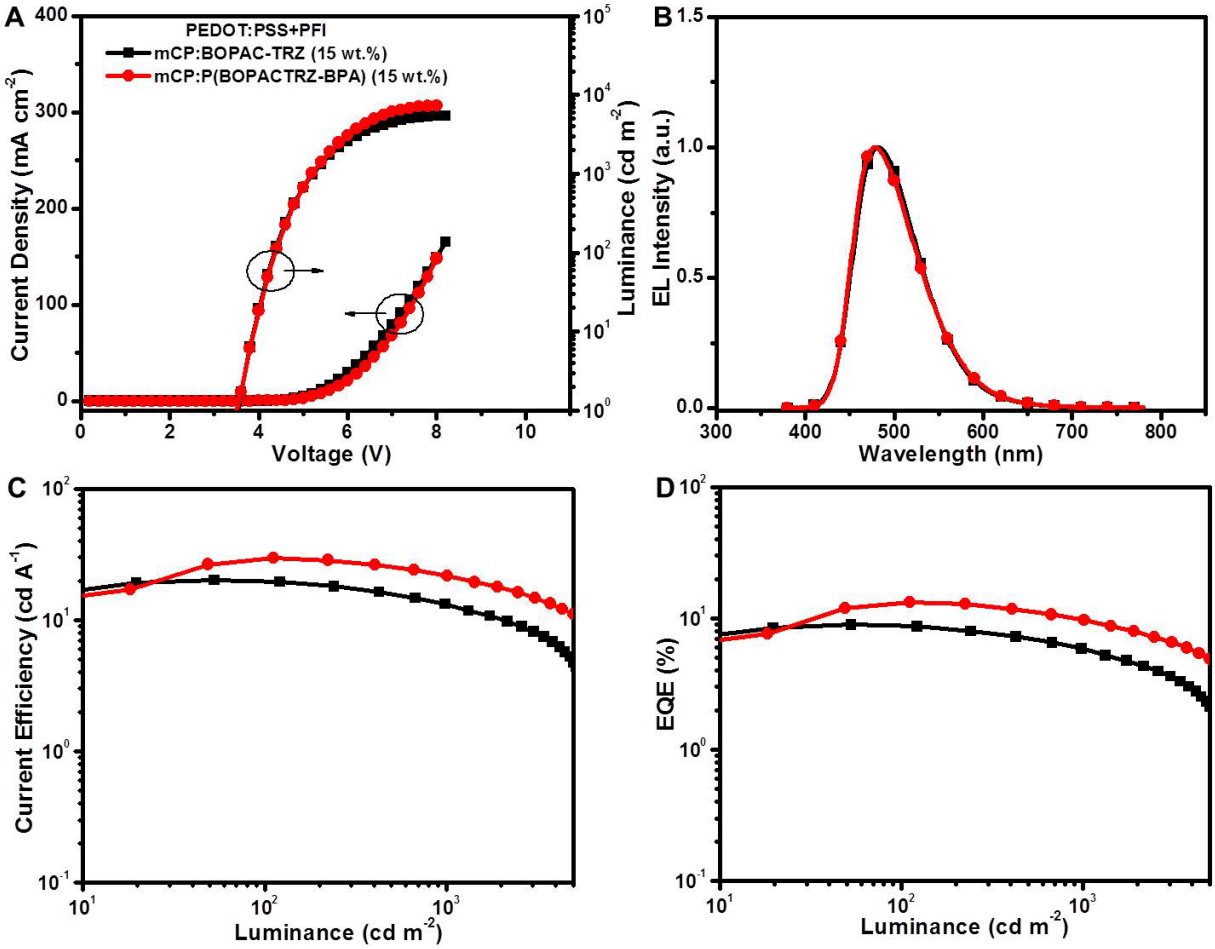


**Figure S10. Performance comparation of BOPAC-TRZ and P(BOPACTRZ-BPA) based blue devices with a doping concentration of 15 wt.% in mCP host and PEDOT:PSS+PFI (v/v 3:2) as the hole-injection layer:** (**A**) current density-voltage-luminance characteristics; (**B**) EL spectrum at a driving voltage of 6 V; (**C**) current efficiency as a function of luminance; (**D**) EQE as a function of luminance. Related to Figure 5 and Table 2.

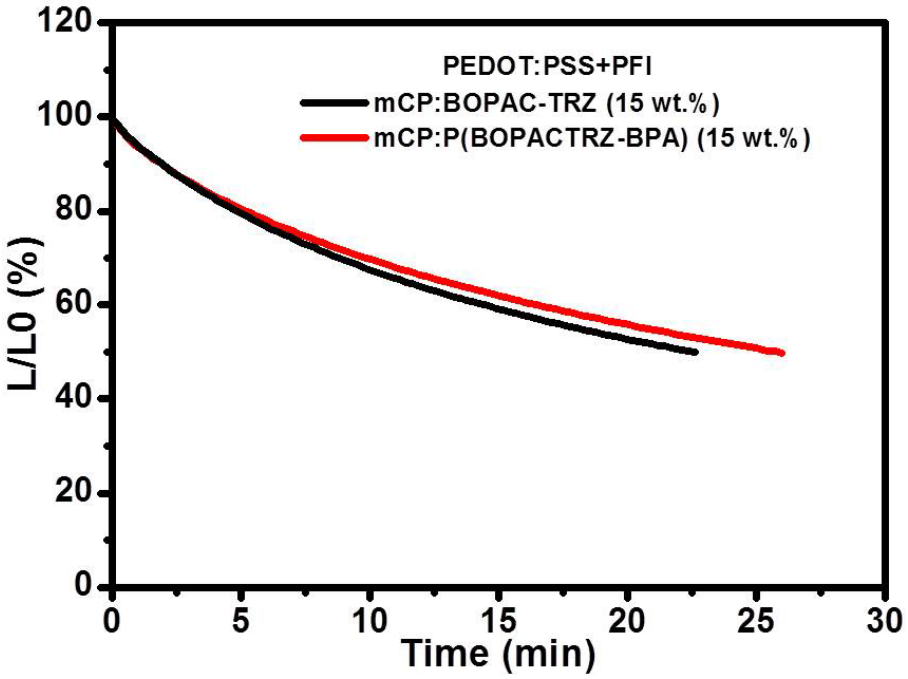


**Figure S11. Lifetime curves of BOPAC-TRZ and P(BOPACTRZ-BPA) based blue devices with a doping concentration of 15 wt.% in mCP host and PEDOT:PSS+PFI (v/v 3:2) as the hole-injection layer.** Lifetime was measured at initial luminance of 100 cd/m$^2$.

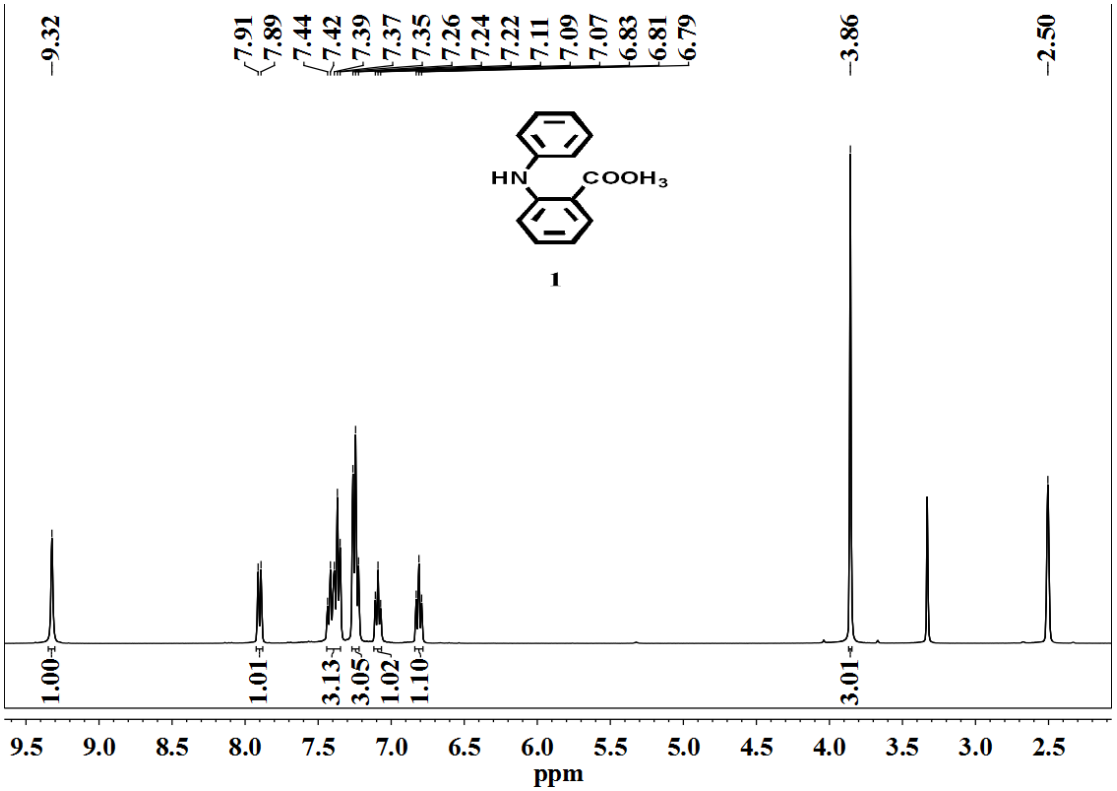


**Figure S12. $^{1}$H NMR spectrum of 1.** Related to Figure 1.

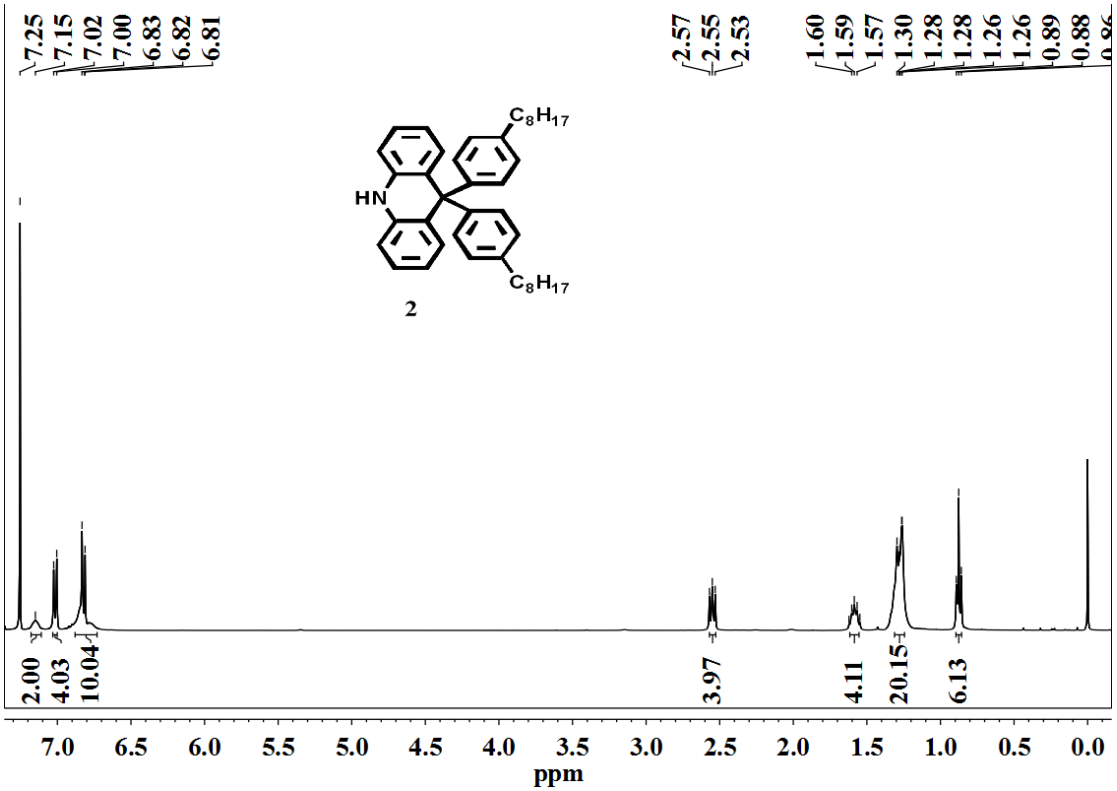


**Figure S13. $^{1}$H NMR spectrum of 2.** Related to Figure 1.

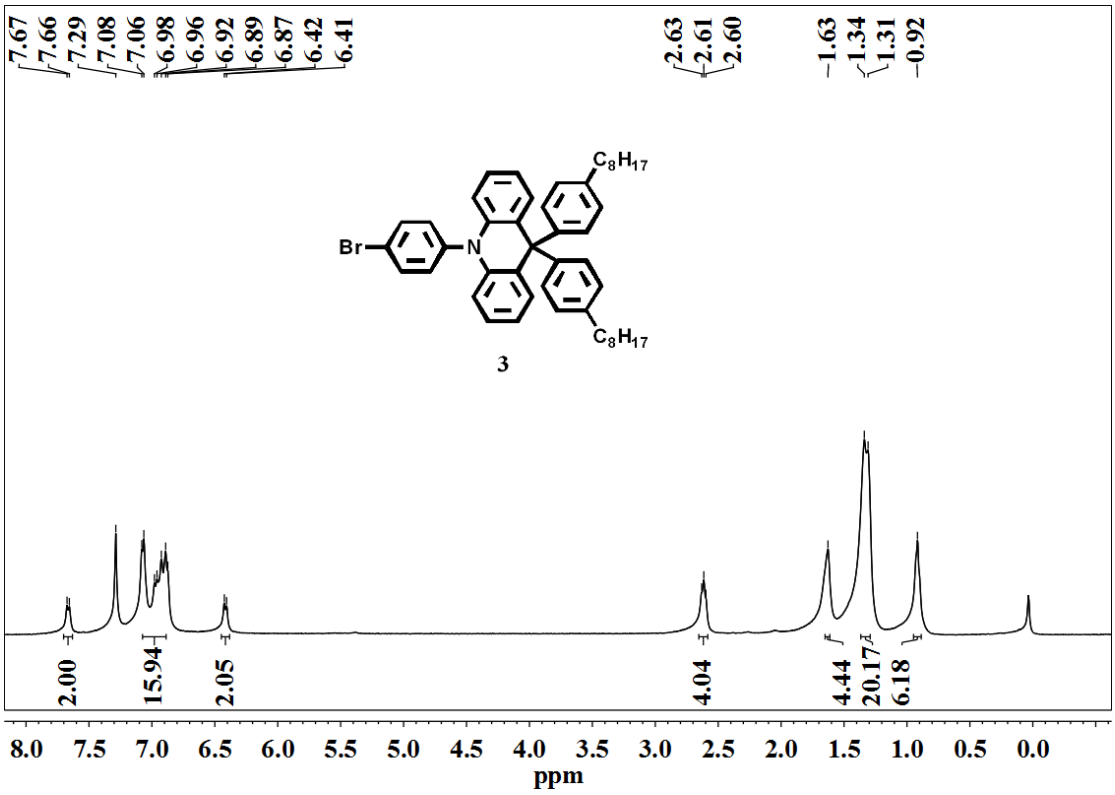


**Figure S14. $^{1}$H NMR spectrum of 3.** Related to Figure 1.

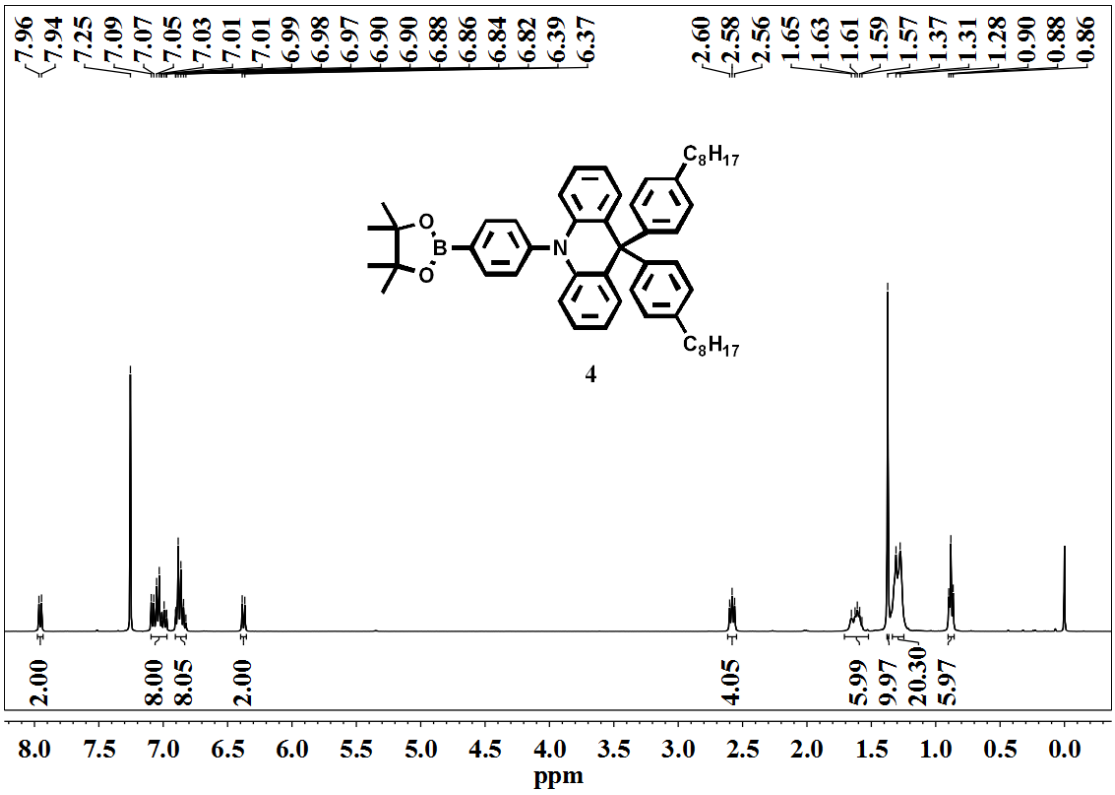


**Figure S15. $^{1}$H NMR spectrum of 4.** Related to Figure 1.

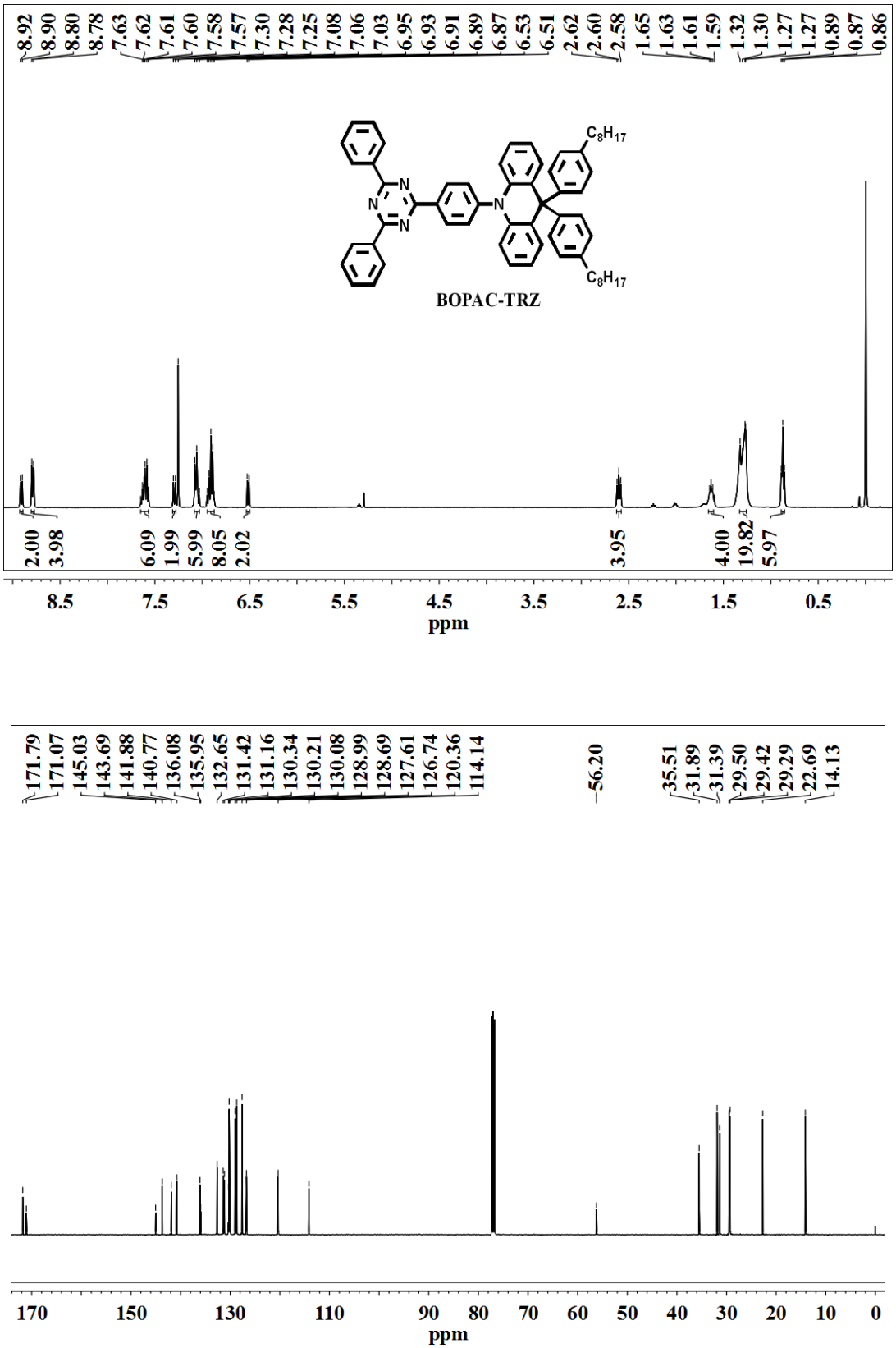


**Figure S16. $^{1}$H and $^{13}$C NMR spectra of BOPAC-TRZ**. Related to Figure 1.

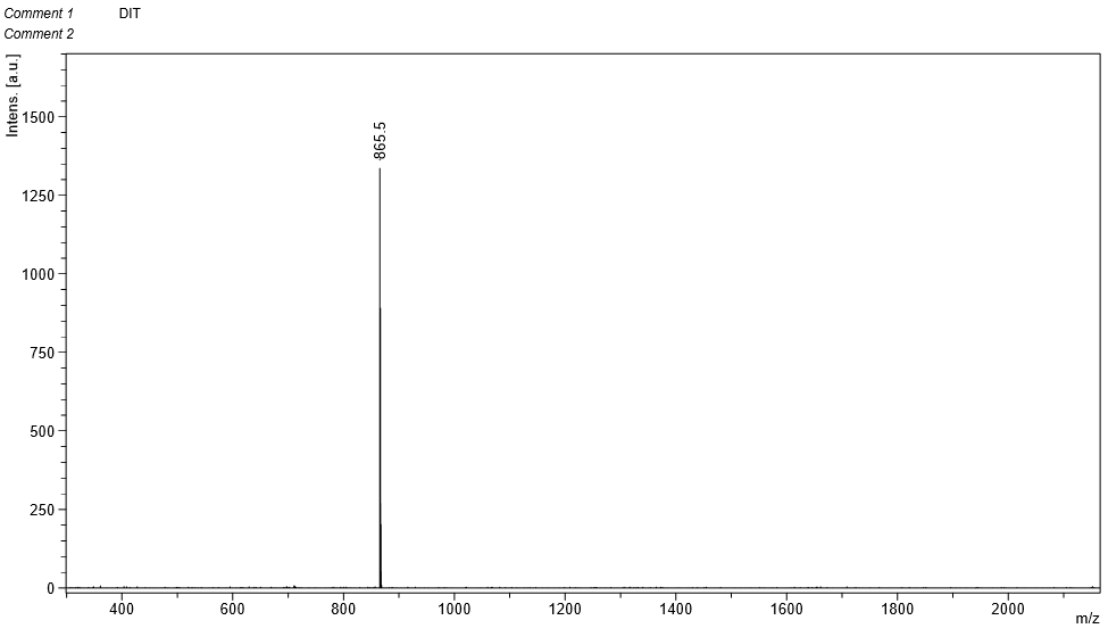


**Figure S17. MALDI-TOF MS spectrum of BOPAC-TRZ.** Related to Figure 1.

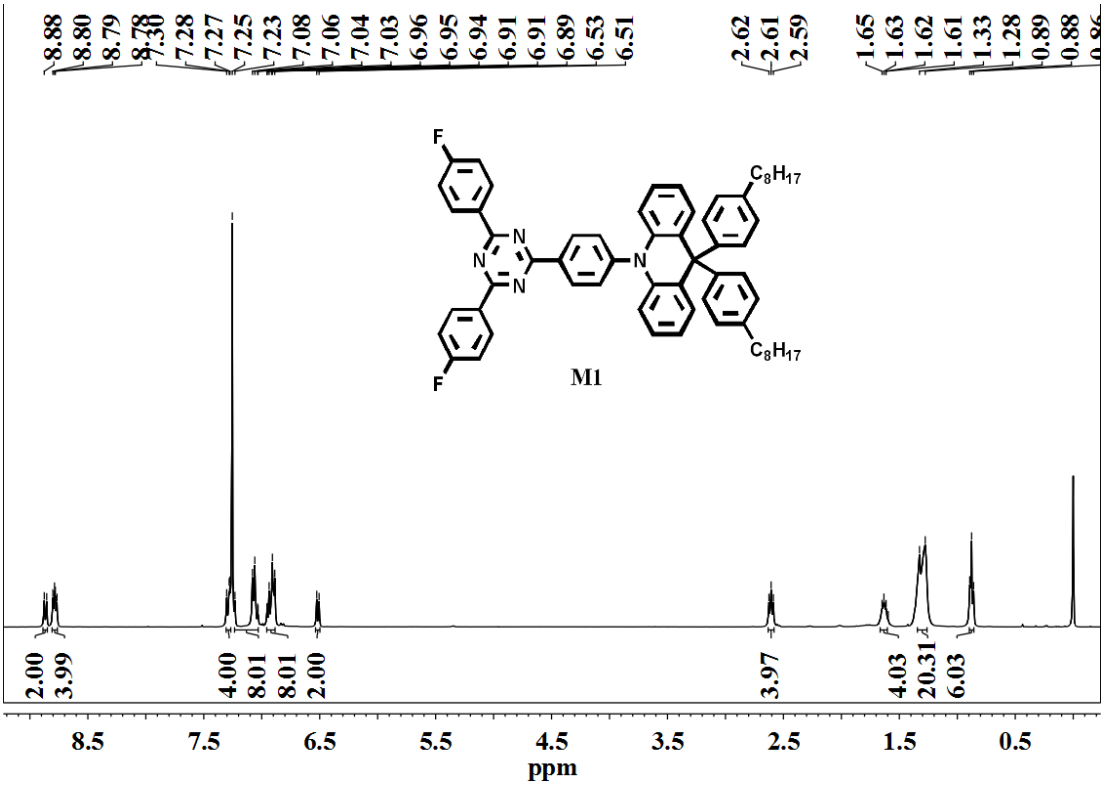


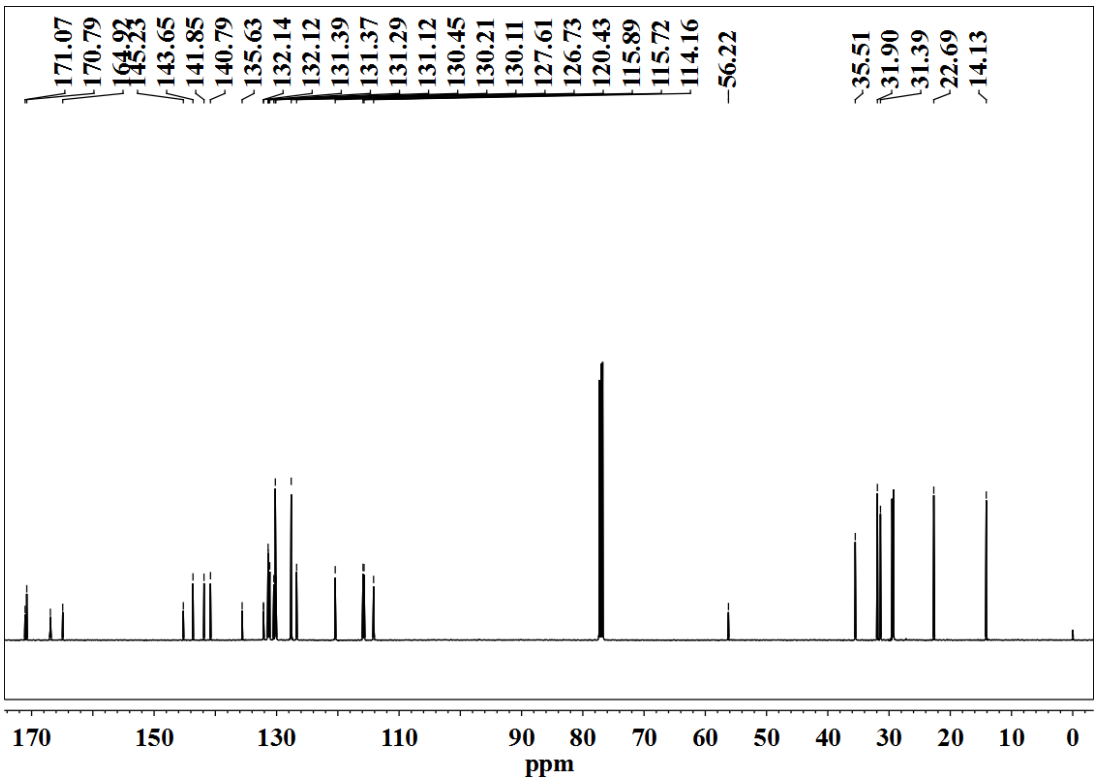


**Figure S18. $^{1}H$ and $^{13}C$ NMR spectra of M1.** Related to Figure 1.

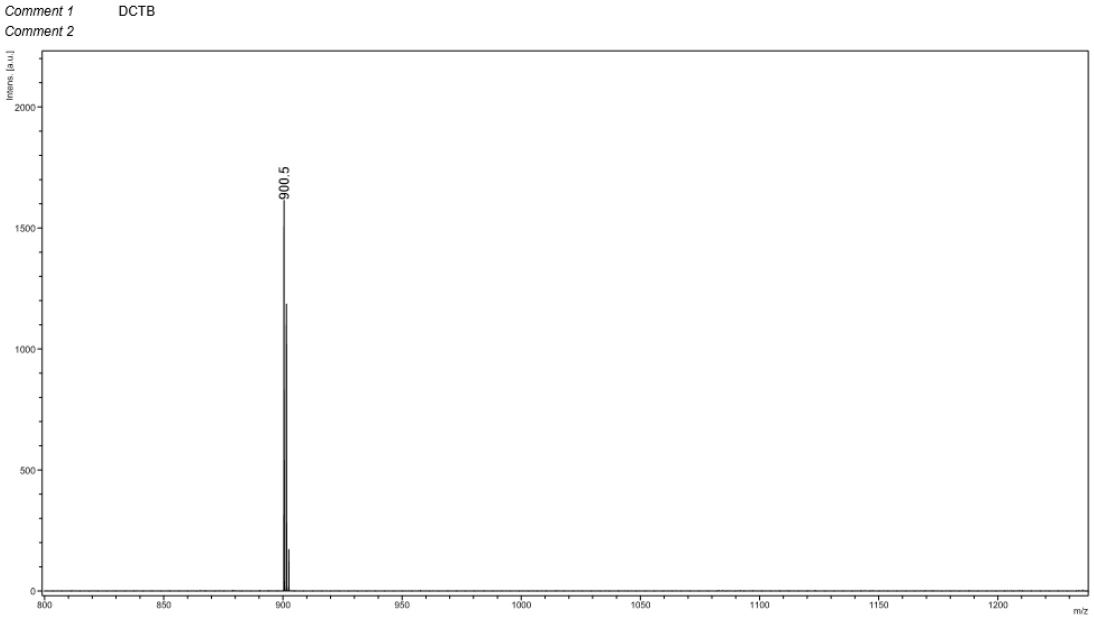


**Figure S19. MALDI-TOF MS spectrum of M1.** Related to Figure 1.

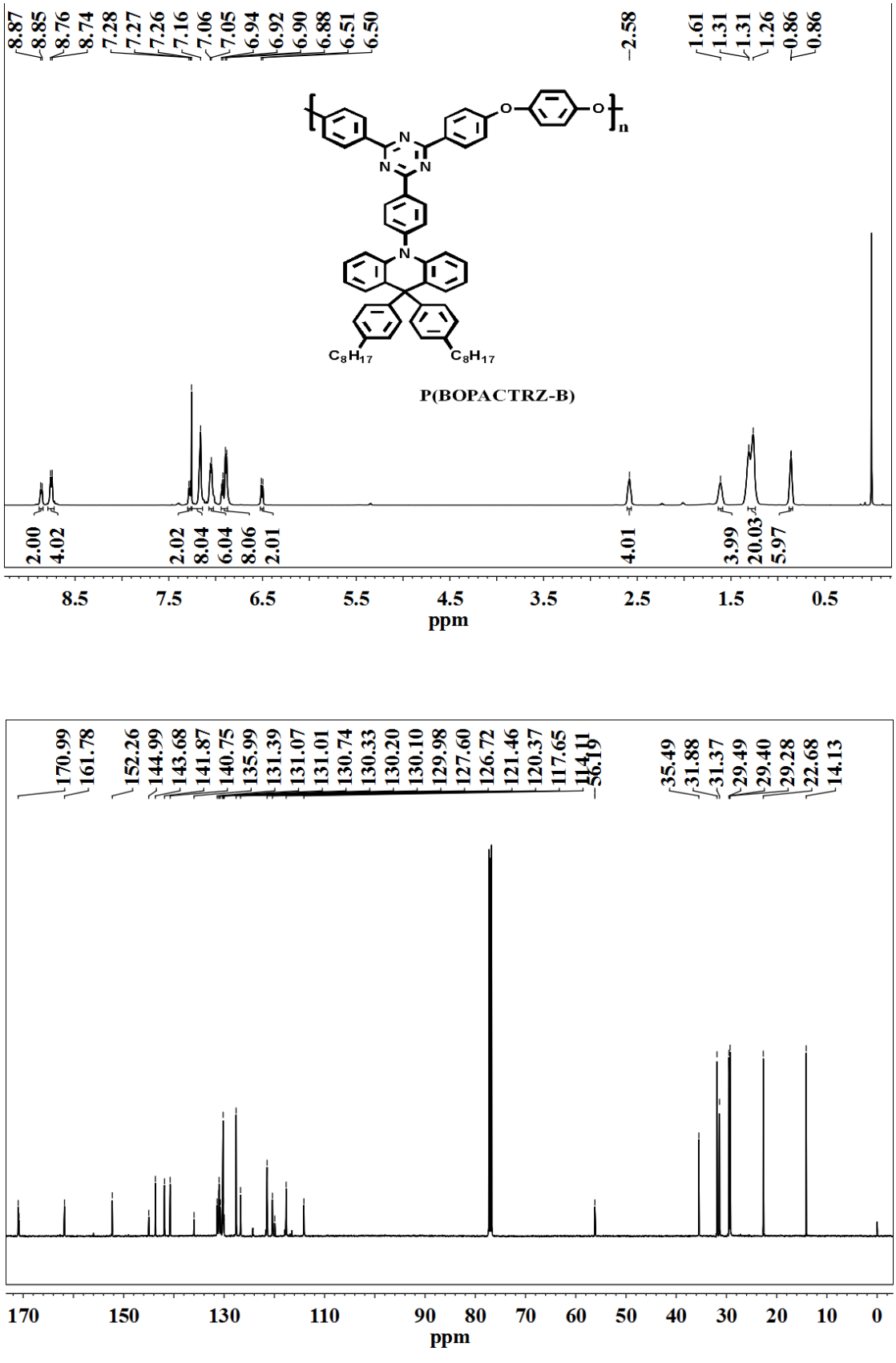


**Figure S20. $^{1}H$ and $^{13}C$ NMR spectra of P(BOPACTRZ-B).** Related to Figure 1.

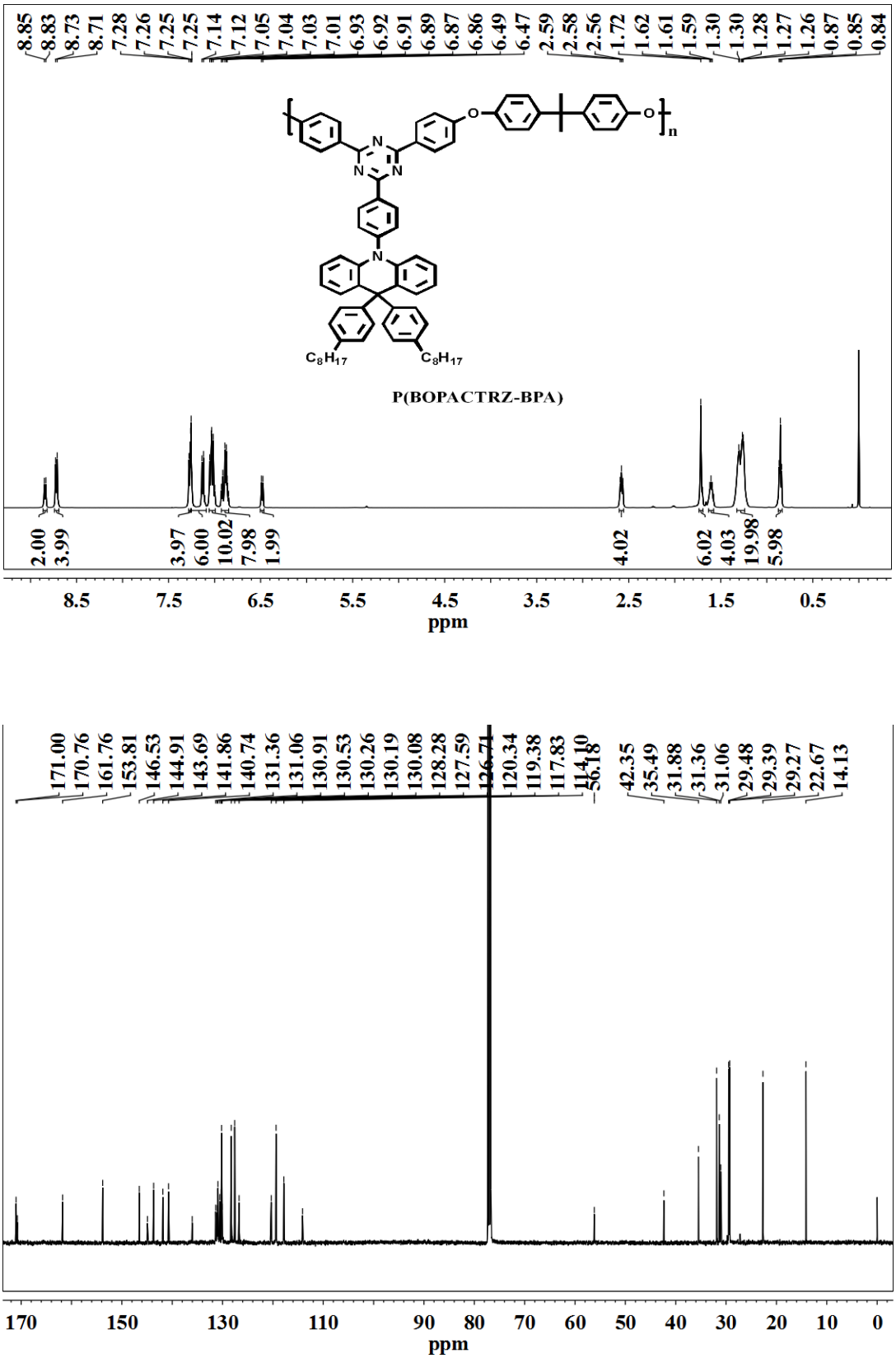


**Figure S21. $^{1}H$ and $^{13}C$ NMR spectra of P(BOPACTRZ-BPA).** Related to Figure 1.

**Supplemental Tables**

**Table S1. Photophysical properties of BOPAC-TRZ, P(BOPACTRZ-B) and P(BOPACTRZ-BPA).** Related to Figure 3 and Table 1.

| Compound | $\tau_p$ (ns) | $\tau_d$ (ns) | $\Phi_p$/ $\Phi_d$/ $\Phi_{PL}$ (%) | $k_p$ ($10^7$ $s^{-1}$) | $k_d$ ($10^5$ $s^{-1}$) | $k_r^S$ ($10^7$ $s^{-1}$) | $k_{ISC}$ ($10^7 s^{-1}$) | $k_{RISC}$ ($10^5$ $s^{-1}$) | $k_{nr}^T$ ($10^5$ $s^{-1}$) |
|---|---|---|---|---|---|---|---|---|---|
| BOPAC-TRZ | 25.2 | 1654.4 | 50.6/24.9/75.5 | 3.97 | 6.04 | 2.01 | 1.96 | 6.02 | 2.99 |
| P(BOPACTRZ-B) | 19.7 | 1172.4 | 34.7/9.8/44.5 | 5.08 | 8.33 | 1.76 | 3.32 | 3.59 | 7.08 |
| P(BOPACTRZ-BPA) | 21.8 | 1623.5 | 49.7/25.6/75.3 | 4.59 | 6.16 | 2.28 | 2.31 | 6.30 | 3.03 |

The related parameters are calculated according to the literatures (*Nature Photon.* **2012,** *6*, 253; *Org. Electron.* **2013**, *14*, 2721). The prompt ($\Phi_p$) and delayed ($\Phi_d$) fluorescence quantum yields are determined by the ratio of emission area in the transient PL spectra based on total PLQY ($\Phi_{PL}$). The prompt ($\tau_p$) and delayed ($\tau_d$) fluorescence lifetimes are obtained following a biexponential fitting. The prompt fluorescence decay rate constant ($k_p$), delayed fluorescence decay rate constant($k_d$), the radiative decay rate constant of the lowest singlet excited state $S_1$ ($k_r^S$), the non-radiative decay rate constant of the lowest triplet excited state $T_1$ ($k_{nr}^T$), the rate constant for intersystem crossing (ISC) from $S_1$ to $T_1$ ($k_{ISC}$), and the rate constant for reverse intersystem crossing (RISC) from $T_1$ to $S_1$ ($k_{RISC}$) are calculated using the following equations:

$k_p = 1/\tau_p$ $\quad$ $k_d = 1/\tau_d$ $\quad$ $k_r^S = k_p \cdot \Phi_p$

$k_{ISC} = k_p \cdot (1-\Phi_p)$ $\quad$ $k_{RISC} = (k_p \cdot k_d / k_{ISC}) \cdot (\Phi_d/\Phi_p)$ $\quad$ $k_{nr}^T = k_d - k_{RISC} \cdot \Phi_p$

**Table S2. Device performance for blue TADF and phosphorescent polymers.**

Related to Figure 5 and Table 2.

| Emitter | CIE (x, y) | $\eta_c$ (cd/A) | $\eta_p$ (lm/W) | EQE (%) | Ref. |
|---|---|---|---|---|---|
| **Blue TADF polymers** | | | | | |
| P(BOPACTRZ-BPA) | (0.18,0.32) | 29.7 | 21.2 | 13.2 | This work |
| P-Ac95-TRZ05 | (0.18,0.27) | 24.8 | - | 12.1 | Shao et al., 2017 |
| PBD-10 | (0.20,0.29) | 13.5 | - | 7.3 | Zeng et al., 2018 |
| **Blue phosphorescent polymers** | | | | | |
| BPP | - | 5.5 | - | 6.6 | Tokito et al., 2003 |
| CP4 | (0.23,0.43) | 2.23 | - | - | You et al., 2006 |
| PCzSiIr5 | - | 2.3 | - | - | Fei et al., 2010 |
| PCbzG1 | (0.18,0.16) | 0.2 | 0.1 | 0.2 | Jin et al., 2011 |
| PB-0.05 | (0.18,0.33) | 19.4 | 10.0 | 9.0 | Shao et al., 2012 |
| PCztPSiB5 | (0.23,0.33) | 3.45 | 1.78 | 1.75 | Xu et al., 2014 |
| P-B-3 | (0.19,0.38) | 15.22 | 12.64 | 6.22 | Liu et al., 2017 |

**Table S3. Performance comparation of BOPAC-TRZ and P(BOPACTRZ-BPA) based blue devices with a doping concentration of 15 wt.% in mCP host and PEDOT:PSS+PFI (v/v 3:2) as the hole-injection layer.** Related to Figure 5 and Table 2.

| Device | $V_{on}$[a] (V) | $L_{max}$ (cd/m$^2$) | $\eta_c$[b] (cd/A) | $\eta_p$[b] (lm/W) | EQE[b] (%) | CIE (x, y) | $T_{50}$[c] (min) |
|---|---|---|---|---|---|---|---|
| mCP:BOPAC-TRZ (15 wt.%) | 3.6 | 5461 | 20.2/18.0/11.8 | 15.1/12.3/6.9 | 8.9/8.0/5.2 | (0.18, 0.32) | 22.6 |
| mCP:P(BOPACTRZ-BPA) (15 wt.%) | 3.6 | 7270 | 29.7/28.7/21.8 | 21.2/19.6/13.2 | 13.2/12.8/9.7 | (0.18, 0.32) | 26.0 |

[a]Turn-on voltage at 1 cd/m$^2$.

[b]Data at maximum, 200 cd/m$^2$ and 1000 cd/m$^2$ for current efficiency ($\eta_c$), power efficiency ($\eta_p$) and EQE, respectively.

[c]The device lifetime measured with an initial luminance ($L_0$) of 100 cd m$^{-2}$.

**Supplemental References**

Shao, S., Hu, J., Wang, X., Wang, L., Jing, X., and Wang, F. (2017). Blue thermally activated delayed fluorescence polymers with nonconjugated backbone and through-space charge transfer effect. J. Am. Chem. Soc. *139*, 17739-17742.

Zeng, X., Luo, J., Zhou, T., Chen, T., Zhou, X., Wu, K., Zou, Y., Xie, G., Gong, S., and Yang, C. (2018). Using ring-opening metathesis polymerization of norbornene to construct thermally activated delayed fluorescence polymers: high-efficiency blue polymer light-emitting diodes. Macromolecules *51*, 1598-1604.

Tokito, S., Suzuki, M., and Sato, F. (2003). Improvement of emission efficiency in polymer light-emitting devices based on phosphorescent polymers. Thin Solid Films *445*, 353-357.

You, Y., Kim, S. H., Jung, H. K., and Park, S. Y. (2006). Blue electrophosphorescence from iridium complex covalently bonded to the poly(9-dodecyl-3-vinylcarbazole): suppressed phase segregation and enhanced energy transfer. Macromolecules *39*, 349-356.

Fei, T., Cheng, G., Hu, D., Dong, W., Lu, P., and Ma, Y. (2010). Iridium complex grafted to 3,6-carbazole-alt-tetraphenylsilane copolymers for blue electrophosphorescence. J. Polym. Sci., Part A: Polym. Chem. *48*, 1859-1865.

Jin, H., Zhang, W., Wang, D., Chu, Z., Shen, Z., Zou, D., Fan, X., and Zhou, Q. (2011). Dendron-Jacketed electrophosphorescent copolymers: improved efficiency and tunable emission color by partial energy transfer. Macromolecules *44*, 9556-9564.

Shao, S., Ding, J., Wang, L., Jing, X., and Wang, F. (2012). Highly efficient blue electrophosphorescent polymers with fluorinated poly(arylene ether phosphine oxide) as backbone. J. Am. Chem. Soc. *134*, 15189-15192.

Xu, F., Kim, J. H., Kim, H. U., Jang, J. H., Yook, K. S., Lee, J. Y., and Hwang, D. H. (2014). Synthesis of high-triplet-energy host polymer for blue and white electrophosphorescent light-emitting diodes. Macromolecules *47*, 7397-7406.

Liu, B., Dang, F., Tian, Z., Feng, Z., Jin, D., Dang, W., Yang, X., Zhou, G., and Wu, Z. (2017). High triplet energy level achieved by tuning the arrangement of building blocks in phosphorescent polymer backbones for furnishing high electroluminescent performances in both blue and white organic light-emitting devices. ACS Appl. Mater. Interfaces *9*, 16360-16374.